Primordial and recycled sulfur sampled by the Iceland mantle plume

Eemu Ranta[1*], Jóhann Gunnarsson-Robin[1], Sæmundur A. Halldórsson[1], Shuhei Ono[2], Gareth Izon[2], Matthew G. Jackson[3], Callum D.J. Reekie[4], Frances E. Jenner[5], Guðmundur H. Guðfinnsson[1], Ólafur P. Jónsson[1], Andri Stefánsson[1]

[1]*Nordic Volcanological Center, Institute of Earth Sciences, University of Iceland, Iceland*
[2]*Department of Earth, Atmospheric and Planetary Sciences, Massachusetts Institute of Technology, USA*
[3]*Department of Earth Science, University of California, Santa Barbara, USA*
[4]*Department of Earth Sciences, University of Cambridge, UK*
[5]*School of Environment, Earth and Ecosystem Sciences, The Open University, UK*

*Corresponding author: Eemu Ranta, eemu@hi.is

ABSTRACT

Stable sulfur isotope ratios of mid-ocean ridge and ocean island basalts (MORBs and OIBs) preserve unique information about early Earth processes and the long-term volatile cycles between Earth's mantle and the surface. Icelandic basalts present ideal material to examine the oldest known terrestrial mantle reservoir, accessed through a deep-rooted mantle plume, but their multiple sulfur isotope systematics have not been explored previously. Here, we present new sulfur concentration (30-1570 ppm), speciation ($S^{6+}/\Sigma S = 0.05–0.43$) and isotope data ($\delta^{34}S_{S^{2-}} = –2.5$ to +3.8 ‰ and $\Delta^{33}S_{S^{2-}} = –0.045$ to +0.016 ‰; vs. Cañon Diablo Troilite) from a large sample suite (N = 62) focused on subglacially erupted basaltic glasses obtained from Iceland's neovolcanic zones. Using these data along with trace element systematics to account for the effects of crustal magmatic processing (degassing and immiscible sulfide melt formation) on $\delta^{34}S$, it is shown that primitive (MgO > 6 wt.%), undegassed glasses accurately record the $\delta^{34}S$ signatures of their mantle sources. Compared to the depleted MORB source mantle (DMM; $\delta^{34}S_{S^{2-}} = –1.3±0.3$ ‰), the Iceland mantle is shown to have a greater range of $\delta^{34}S_{S^{2-}}$-values between –2.5 and –0.1%. Similarly, Icelandic basalts are characterized by more variable and negatively shifted $\Delta^{33}S$ values (–0.035 to +0.013 ‰) relative to DMM (0.004±006 ‰). Negative $\delta^{34}S$ and $\Delta^{33}S$ signatures are most prominent in basalts from the Snæfellsnes Volcanic Zone and the Kverkfjöll volcanic system, which also have the lowest, most MORB-like $^3He/^4He$ (8–9 R/R_A, where R_A is the $^3He/^4He$ of air) and the highest Ba/La (up to 12) in Iceland. We propose that subduction fluid-enriched, mantle wedge type material in the North Atlantic upper mantle constitutes a low-$\delta^{34}S$-$\Delta^{33}S$ component in the Icelandic mantle. This suggests that volatile heterogeneity in Iceland, and potentially at other OIBs, may originate not only from diverse plume-associated mantle components, but also from a heterogeneous ambient upper mantle. By contrast, a set of samples with high $^3He/^4He$ (up to 25.9 R/R_A) and negative $\mu^{182}W$ anomalies define a primordial lower mantle reservoir with a near-chondritic $\delta^{34}S_{\Sigma S}$ and $\Delta^{33}S$ signature of ~0 ‰. This sulfur isotopic signature is difficult to reconcile with the non-chondritic sulfur isotopic signature of the DMM and may reflect either separate conditions during core formation, or a previously unidentified flux of sulfur from the core to the high-$^3He/^4He$ reservoir.

Keywords: sulfur isotopes, ocean island basalts, Iceland, deep volatile recycling, primordial mantle, core-mantle interaction

1 INTRODUCTION

Mass-independent S isotope fractionation signatures (S-MIF; $\Delta^{33}S \neq 0$) measured in sulfides from the South Pacific Pitcairn and Mangaia hotspots provide remarkable evidence for the resurfacing of Archean sedimentary material through ocean island basalts (OIBs) (Cabral et al. 2013; Delavault et al. 2016). By contrast, the depleted upper mantle (DMM) as sampled by mid-ocean ridge basalts (MORBs) features chondritic $\Delta^{33}S$ values (~0‰) coupled with a sub-chondritic $\delta^{34}S$ signature (–1.28±0.33‰; Labidi et al. 2013), which requires that ~97% of Earth's sulfur partitioned to the core during core-mantle differentiation (Labidi et al. 2013, 2016; Labidi and Cartigny 2016). Determining the multiple sulfur isotopic composition of high-$^{3}He/^{4}He$ OIBs, which are thought to tap primordial lower mantle reservoirs (Yuan and Romanowicz 2017; Mundl-Petermeier et al. 2020), could provide additional constraints on the timing and nature of Early Earth processes, but to date, published data are limited to two highly degassed high-$^{3}He/^{4}He$ samples from Samoa (Dottin et al. 2020a).

The mantle plume beneath Iceland samples what is thought to be the oldest and most primordial material available on Earth, i.e., a part of the deep mantle that has remained unstirred by mantle processes since at least 4.45 Ga. Such ancient origin is supported by ^{129}Xe-excesses that could have been generated only in the earliest Hadean (Mukhopadhyay 2012), the highest modern terrestrial mantle $^{3}He/^{4}He$ values (Harðardóttir et al. 2018) and negative $\mu^{182}W$ anomalies (Mundl-Petermeier et al. 2019). Nevertheless, spatial co-variation between isotopic and trace element source indicators hints toward a heterogeneous Icelandic mantle, comprising one or more recycled components and ambient upwelling DMM in addition to the high-$^{3}He/^{4}He$ component (Hanan et al. 2000; Macpherson et al. 2005; Halldórsson et al. 2016a,b; Harðardóttir et al. 2018; Rasmussen et al. 2020). Due the unique dual role of sulfur as a volatile element in near-surface processes, and its strong partitioning to the core during core-mantle differentiation, the $\delta^{34}S$ and $\Delta^{33}S$ composition of Icelandic basalts could provide unique constraints on both the early planetary history of Earth and the deep recycling of sulfur through the mantle.

Previously published $\delta^{34}S$ values for Icelandic basalts range from –2.0 to 0.4‰ (Torssander 1989), but are difficult to interpret in terms of source values due to their highly degassed nature. In this study, we combine a newly developed HF extraction protocol (Labidi et al. 2012) with improved mass spectroscopy (Ono et al. 2006) to generate a high precision quadruple sulfur isotope dataset (^{32}S, ^{33}S, ^{34}S and ^{36}S) measured from dissolved sulfide (S^{2-}) in a large set of subglacial basaltic glasses. Importantly, our subglacial glass samples are largely devoid of secondary $\delta^{34}S$ shifts imposed by degassing and assimilation of seawater-derived sulfate. Instead, the data illuminate the effects of immiscible sulfide melt formation during crustal magmatic evolution on both sulfur speciation ($S^{6+}/\Sigma S$) and $\delta^{34}S$ of dissolved sulfide ($\delta^{34}S_{S^{2-}}$), and enables us to constrain the $\delta^{34}S$ and $\Delta^{33}S$ signatures of distinct mantle components beneath Iceland.

2 SAMPLES & METHODS

2.1 Samples

Our sample set (n = 62) focuses on Pleistocene subglacial glasses (n = 59; Fig. 1) that represent most of the geochemical range of Icelandic magma series, encompassing rhyolites, andesites and basalts (0.1–9.9 wt.% MgO; Fig. 2). The samples cover the main on-land rift zones of Iceland, comprising the Northern, Western and Eastern Rift Zones (NRZ, WRZ and ERZ, respectively), as well as the propagating rift of South Iceland Volcanic Zone (SIVZ) and the off-rift Snæfellsnes Volcanic Zone (SNVZ) (Fig. 1). The rift zone lavas are tholeiitic, while the SIVZ and SNVZ lavas are transitional to alkaline. To assess the sulfur isotope systematics of a single magmatic lineage, 15 samples were included from the Kverkfjöll volcanic system, located in the south-eastern flank of the NRZ.

Most subglacial glasses (n = 45) were quenched under sufficiently high pressure to prevent significant S degassing (Supplementary Information). Moreover, the potential effect of crustal assimilation on S isotopic compositions of Icelandic basalts is likely to be small because of the higher S content of deep, undegassed melts (400-1600 ppm) relative to hydrothermally altered crust which is expected to be S-depleted due to degassing and leaching of sulfur by hydrothermal fluids (Alt et al. 1995; Gunnarsson-Robin et al. 2017). An additional advantage of the subglacial glasses is that they are unaffected by assimilation of seawater sulfate-derived S, a process which is known to increase both measured S concentrations and $\delta^{34}S$ values in submarine pillow glasses (Labidi et al. 2014). Absence of seawater-influence in Icelandic subglacial basalts is demonstrated by lack of elevated Cl/K ratios above ~0.10 (Halldórsson et al. 2016a). Thus, subglacial glasses closely capture the pre-eruptive melt compositions with respect to S concentrations and isotope ratios, presenting a significant advantage over the subaerial samples targeted in the only previous sulfur isotope appraisal in Iceland (Fig. 2a; Torssander, 1989) and many previous sulfur isotope studies on

OIBs (e.g., Dottin et al. 2020a). Three subaerial lavas (A-THO, B-ALK, I-ICE) are included to examine the effect of near-surface degassing on S concentration, $S^{6+}/\Sigma S$ and $\delta^{34}S$.

2.2 Major and trace elements and sulfur speciation

Major element content, S concentrations and S speciation in the glasses were determined by electron probe microanalysis (EPMA) at the Institute of Earth Sciences, University of Iceland. Trace element analysis was performed using inductively coupled plasma mass spectrometry (ICP-MS) at the Scripps Institution of Oceanography, as well as laser ablation ICP-MS (LA-ICP-MS) at the Research School of Earth Sciences, Australian National University and at the Geological Survey of Finland. Additional details on analytical protocols are provided in the Supplementary Information.

2.3 Sulfur extraction protocol

Sulfur was extracted from powdered hand-picked glasses or rock fragments and converted to $Ag_2S(s)$ via the coupled HF dissolution/Cr reduction method using an all-teflon extraction line (Labidi et al. 2012). The dissolved S^{2-} was released as $H_2S(g)$ and flushed within a nitrogen stream via a water trap before being precipitated as $Ag_2S(s)$ in a $AgNO_3$ trapping solution. The resultant $Ag_2S(s)$ was heated at 80 °C for 3-6 hours, cleaned in triplicate using deionized water (18.2 MΩ·cm) prior to being dried and weighed. Gravimetric extraction yields were calculated relative to the EPMA-derived S concentrations, and were found to vary between 60 and 110%. Rather than incomplete extractions, this relatively large spread in yields probably reflects a combination of variable crystal content and $S^{6+}/\Sigma S$ of the extracted material (Supplementary Information). Importantly, no relationship between yields and measured S isotope values was identified (Fig. S1). Repeated extractions of the relatively aphyric glass STAP-1, with a measured $S^{6+/}\Sigma S$ of 0.22±0.03, returned an average yield of 91±11 % (1σ, n = 10).

2.4 Sulfur isotope analysis

Sulfur isotope ratios were determined via dual-inlet isotope ratio mass spectrometry (IRMS) at the Stable Isotope Geobiology Laboratory at the Massachusetts Institute of Technology (MIT) following the methodology described by Ono et al. (2006, 2012). Here, approximately

2 mg of Ag_2S was converted into $SF_6(g)$ via overnight reaction with $F_2(g)$ at 300°C. The resultant $SF_6(g)$ was initially purified cryogenically before being isolated by preparative tandem-column (molecular sieve 5 Å and HayesepQ) gas chromatography. The purified analyte was introduced to a Thermo Scientific MAT 253 IRMS instrument where the mass/charge ratios 127, 128, 129, 131, corresponding to $^{32,33,34,36}SF_5^+$ ions, were measured. The $^{34}S/^{32}S$ data are reported in δ-notation relative to the Vienna Cañon Diablo Troilite (VCDT), following:

$$\delta^{34}\mathrm{S}_{\mathrm{sample}} = \frac{\left(^{34}\mathrm{S}/^{32}\mathrm{S}\right)_{\mathrm{sample}} - \left(^{34}\mathrm{S}/^{32}\mathrm{S}\right)_{\mathrm{VCDT}}}{\left(^{34}\mathrm{S}/^{32}\mathrm{S}\right)_{\mathrm{VCDT}}} \qquad (1)$$

The VCDT scale is defined by the IAEA-S-1 standard with a $\delta^{34}S_{VCDT}$ value of -0.3 ‰ (Coplen and Krouse, 1998). Deviation from a mass-dependent fractionation line is reported in Δ notation as

$$\Delta^{x}\mathrm{S} = \ln(\delta^{x}\mathrm{S} + 1) - \theta^{x}\ln(\delta^{34}\mathrm{S} + 1) \qquad (2)$$

where x = 33 or 36, $\theta^{33} = 0.515$ and $\theta^{36} = 1.90$. Replicate analyses of an in-house Ag_2S standard (Ono-Ag2S), the IAEA-S-1 reference material and three subglacial glasses are reported in Tables S1 and S2. Based on 18 analyses of Ono-Ag_2S during our sessions, long-term $\delta^{34}S$, $\Delta^{33}S$ and $\Delta^{36}S$ reproducibilities are estimated at 0.12, 0.004, and 0.086 ‰ (all 1σ), respectively (Fig. S1). Repeat measurements of IAEA-S-1 yield respective $\delta^{34}S$, $\Delta^{33}S$ and $\Delta^{36}S$ values of -1.19±0.17 ‰, +0.100±0.004 ‰ and -0.669±0.068 ‰, relative to the MIT reference gas SG1 (Table S-1). Given the lack of reference materials with certified $\Delta^{33}S_{CDT}$ and $\Delta^{36}S_{CDT}$ values, different laboratories have defined the CDT-scale via measurements of IAEA-S-1 and CDT (Table S3, Fig. S2). Because no CDT measurements have been conducted at the MIT lab, we anchor the CDT scale by defining the respective $\Delta^{33}S_{CDT}$ and $\Delta^{36}S_{CDT}$ values of IAEA-S-1 as +0.109 and –0.730 ‰, which represents the average of previously established IAEA-S-1 values (Supplementary Information). This makes it possible to compare our dataset with previously published multiple sulfur isotope datasets for MORBs and OIBs.

The relatively large uncertainty associated with $\Delta^{36}S$ measurements results from the low natural abundance of ^{36}S (0.015 %) and potential isobaric interferences on mass 131 (Ono et al. 2006). While $\Delta^{36}S$ data is reported for completeness, its large uncertainty relative to the subdued variability within our samples limits its utility beyond that of $\Delta^{33}S$.

3 RESULTS

Sulfur concentration, speciation and isotope data as well as major and trace element abundances are reported in Tables S-4 and S-5.

Sulfur concentrations. The samples (including both subaerial lavas and subglacial glasses) display variable S concentrations from 30 to 1570 ppm. Overall, sulfur concentrations increase from 300-800 ppm in the most primitive subglacial glasses (9-10 wt.% MgO) to a peak of 1200-1570 ppm at 6 wt.% MgO, before decreasing to about 1100 ppm at 4 wt.% MgO (Fig. 2a). Breaks from these trends are seen in a subset of the subglacial glasses, which show marked S depletions at given MgO content (Fig. 2a). Lowest sulfur contents are seen in the subaerial lavas (30 to 70 ppm). The main trend closely follows the pre-eruptive sulfur concentrations as recorded by melt inclusion datasets available for Icelandic basalts (Fig. 2a). Of the other examined trace elements, only Cu shows a similar trend (Fig. 3a). Hereafter, the two distinct melt evolution trends defined by S and Cu are referred to as Phase 1 (MgO > 6 wt.%) and Phase 2 (MgO < 6 wt.%). Sample A36 has anomalously high S and Cu concentrations. Similar over-enrichments in S are recorded by a subset of basaltic melt inclusions (Fig. 2a), which at other localities has been explained by resorption of sulfides (Reekie et al. 2019; Wieser et al. 2020).

Sulfur speciation. The Icelandic glasses we deem to be less affected by degassing (see section 4.1) have $S^{6+}/\Sigma S$ between 0.04 and 0.23 with an average of 0.15±0.05 (1σ, $n = 45$; Fig. 2b). This average value is similar to those reported from Samoan (0.17±0.11; Labidi et al. 2015) and Hawaiian basalts (0.15±0.05 for submarine Kilauea eruption; Jugo et al. 2010) but higher than reported for MORBs (< 0.1; Jugo et al. 2010). This is compatible with the more oxidized nature of OIBs (Jugo et al. 2010). In contrast, the most degassed samples have elevated $S^{6+}/\Sigma S$ of up to 0.43 (Fig. S3). If the degassed samples are removed, two trends emerge: $S^{6+}/\Sigma S$ in primitive melts decreases during melt evolution in Phase 1 from ~0.17 to values of ~0.10 and then increases to ~0.20 during Phase 2 (Fig. 2b).

Sulfur isotopes. The overall variation in $\delta^{34}S_{S^{2-}}$ captured within our Icelandic samples is –2.5 to +3.8‰ (Fig. 4). This range is similar to previously reported $\delta^{34}S$ data for Icelandic lavas (Torssander 1989; Fig. 4a) and exceeds the $\delta^{34}S_{S^{2-}}$ range displayed by MORBs (–1.8 to +1.0, $n = 68$; Labidi and Cartigny 2016 and sources therein). Nevertheless, positive values are clearly linked to degassed samples (Fig. 4a; Section 4.1; Torssander, 1989), while undegassed basaltic glasses display a more limited range of $\delta^{34}S_{S^{2-}}$ values from –2.5 to –0.1 ‰. Thus, Icelandic basalts lack the positive $\delta^{34}S$ values characteristic of OIBs at Samoa (Labidi et al. 2015) and the Canary Islands (Beaudry et al. 2018). The most negative $\delta^{34}S_{S^{2-}}$-values are observed in the most primitive Kverkfjöll basalts NAL-356 (–2.3 ‰) and NAL-585 and (–2.0 ‰) and in the highly primitive (MgO = 9.9 wt.%) and geochemically depleted WRZ sample MID-1 (–2.5 ‰). The $\delta^{34}S_{S^{2-}}$ values generally increase with decreasing MgO, a trend that is most clear in the ERZ and Kverkfjöll sample suites (Fig 4b).

The $\Delta^{33}S$ values of the entire dataset vary between –0.045 and +0.016 ‰, or between –0.035 to +0.010 ‰ (±0.013, 1σ) if subaerial samples are excluded (Fig. 5). The Icelandic glasses have an average $\Delta^{33}S$ value of -0.002±0.010 ‰ (1σ, n = 59) and extend to more negative values compared to Samoan OIBs (0.008±0.007 ‰; 1σ, n = 22; Labidi et al. 2015, Dottin et al. 2020a) and MORBs (0.004±0.006 ‰ (1σ, n = 68; Labidi et al. 2012, 2013, 2014, Labidi and Cartigny 2016; Fig. 5). Although their average $\Delta^{33}S$ values overlap within 1σ, a statistical student's t test indicates that, as a whole, Icelandic basalts reflect a different population from both Samoan OIBs and MORBs (p value < 0.001).

4 DISCUSSION

4.1 Magmatic degassing

Sulfur degassing from low-H_2O basaltic magmas commences at pressures of ~150 MPa (Wallace and Edmonds 2011) and thus, should not have significantly affected the pre-eruptive S inventory of Icelandic basalts, which are typically stored at considerably higher pressures (e.g. Halldórsson et al. 2018). Therefore, any S degassing observed in subglacial glasses is expected to be solely related to eruptive degassing (Figs. 2a and S3; Supplementary Information). Degassing can lead to either positive or negative $\delta^{34}S$ fractionation, expressed as $\varepsilon^{34}S_{\text{gas-melt}}$ (see Eq. 13 for definition; note that ε is used here for the fractionation factor to avoid confusion with Δ, which is used for denoting S-MIF). The sign of $\varepsilon^{34}S_{\text{gas-melt}}$ is determined by the S speciation of the gas and the melt, i.e., SO_2/H_2S(g) and S^{6+}/S^{2-}(m), respectively (Fig. S4; Supplementary Information). For example, the sign of $\varepsilon^{34}S_{\text{gas-melt}}$ is positive during degassing of oxidized gases from reduced melts (high SO_2/H_2S(g) and low S^{6+}/S^{2}(m)), and negative during the converse (low SO_2/H_2S(g) and high S^{6+}/S^{2}(m); Fig. S4). Considering the relatively reduced nature of undegassed Icelandic melts ($S^{6+}/\Sigma S$ =

0.14±0.09), deep degassing (with low $SO_2/(SO_2+H_2S) < 0.4$) at T = 1200 °C only leads to modest $\delta^{34}S$ fractionation of $\varepsilon^{34}S_{gas-melt}$ = 0±0.5‰ (Fig. S4a). Predominance of H_2S in the gas phase is also shown by clearly increased $S^{6+}/\Sigma S$ in the most degassed melts (Fig. S3). Notably, even 30 % degassing is only expected to lead to minor $\delta^{34}S_{melt}$ fractionation of ±0.4 ‰ (Fig. 4a). Therefore, identifying and filtering out samples that have only experienced minor amounts of degassing is not necessary, as they closely record their source $\delta^{34}S$ values.

In contrast, negative $\varepsilon^{34}S_{gas-melt}$ fractionation factor is expected during degassing of more oxidized melts, shifting $\delta^{34}S_{melt}$ toward more positive values. Such clear degassing-induced changes in $\delta^{34}S$ toward more positive values is seen in our most oxidized basaltic sample BOTN-1 ($S^{6+}/\Sigma S = 0.43$) and in the rhyolitic glass A-THO ($S^{6+}/\Sigma S = 0.43$), which are both highly degassed (Fig. 4a). Similarly, the most degassed Icelandic subaerial samples from Torssander (1989) trend toward positive $\delta^{34}S$ values (Fig. 4a). This indicates that in general, S degassing has an oxidizing effect on Icelandic magmas. As the source $\delta^{34}S$ values are not accurately preserved in heavily degassed samples (A1, A3, A6, A32, THOR-1, STORID-1, SELJA-1, SAL-601, BOTN-1, HNAUS-1, OLAF-1, NAL-460, KVK-202, KVK-205), they are filtered out from Figs. 6a, 7a and 8a and are not considered in subsequent discussion on $\delta^{34}S$ signatures.

4.2 Sulfide immiscibility

4.2.1 Quantifying sulfide melt formation

Immiscible sulfide melts effectively sequester S and chalcophile elements, such as Cu, from magmas that are sulfide saturated (Bézos et al. 2005; Jenner et al., 2010, Reekie et al. 2019). The observed trend of decreasing Cu concentrations with decreasing MgO below c. 6 wt.% (Fig. 3a) clearly implicates sequestration of Cu by an immiscible sulfide melt, as has been previously noted in Icelandic whole-rock data (Momme et al. 2003). An analogous trend is observed for S and S/Dy, but is less distinct due to degassing-induced scatter (Figs. 2a and 3c).

The kinks observed at MgO = 6 wt% for Cu, S, Cu/Y and $S^{6+}/\Sigma S$ define the boundary between Phase 1 (between MgO = 6-10 wt.%) and Phase 2 (MgO = 4-6 wt.%; Figs. 2 and 3). Similar phases have been identified for Samoan basalts (Labidi et al., 2015). The weight fraction of fractionated sulfide (X_{sulf}) during both phases can be quantified using

$$X_{\mathrm{sulf}} = \frac{D_{\mathrm{Cu}}^{\mathrm{min-liq}} - D_{\mathrm{Cu}}^{\mathrm{sil-liq}}}{D_{\mathrm{Cu}}^{\mathrm{sulf-liq}} - D_{\mathrm{Cu}}^{\mathrm{sil-liq}}} \tag{3}$$

where $D_{\mathrm{Cu}}^{\mathrm{min-liq}}$, the empirical bulk partition coefficient of Cu between crystallizing minerals and silicate melt, is estimated using the observed Cu trends (see Labidi et al. 2014; Supplementary Information). The partition coefficients of Cu between silicate minerals and silicate melt, $D_{\mathrm{Cu}}^{\mathrm{min-liq}}$, and between sulfide and silicate melts, $D_{\mathrm{Cu}}^{\mathrm{sulf-liq}}$ are taken as 0.1 and 900, respectively (Lee et al. 2012; Labidi et al. 2014). This yields X_{sulf} = 800 ppm for Phase 1 and 2580 ppm for Phase 2 for Icelandic melts. Physical evidence of sulfide saturation during Phase 2 is preserved as Cu-rich sulfide globule inclusions observed in melt inclusions (Fig. S7). However, the apparent early fractionation of sulfides during Phase 1 may be an artefact of the sulfide fractionation model, as the relatively low S contents in Phase 1 melts fall below [SCSS^{2-}] (S concentrations at sulfide saturation; Fig. 2a; Fortin et al., 2015). Alternatively, the lower-than-expected Cu increase and the negatively sloping Cu/Y trend during Phase 1 could be a result of melt-mixing processes (Shorttle and Maclennan 2011).

We interpret these results to show that Icelandic melts become sulfide saturated below MgO = 6 wt.% (cf. Halldórsson et al. 2018). In this respect, Icelandic melts contrast with MORBs, that fractionate sulfides throughout their crustal evolution path (Bézos et al. 2005). Instead, this behavior is more similar to arc magmas, where the onset of magnetite crystallization leads a reduction in melt f_{O_2}, triggering sulfide saturation at about 2-3 wt.% MgO (Jenner et al. 2010), a process also suggested to explain the Cu versus MgO trend observed at Samoa (Labidi et al. 2015). However, in Icelandic magma series the onset of Phase 2 clearly predates the onset of magnetite formation, which is observed only in glasses with MgO < 5 wt.%. A more complex pattern of multiple starts and stops in sulfide saturation during magmatic evolution that are reported for basalts from the Kilauea volcano in Hawaii (Wieser et al., 2020) are not strictly required to explain the Iceland data, although we cannot rule out the possibility that some melts were sulfide saturated at higher pressures and became undersaturated upon ascent to higher level crustal magma chambers (Reekie et al., 2019; Wieser et al., 2020).

4.2.2 Effect of sulfide fractionation on $\delta^{34}S$ evolution of Icelandic basalts

In a non-redox buffered system, sulfide fractionation leads to an increase in the melt $S^{6+}/\Sigma S$ and thereby an increase in melt $\delta^{34}S_{\Sigma S}$ values because S^{6+} is isotopically heavier than S^{2-} ($\varepsilon^{34}S_{\text{sulfate-sulfide}} \approx +3$ ‰ at T = 1250°C). In this case, no change in melt $\delta^{34}S_{S^{2-}}$ values should be observed (Fig. S6; Labidi et al. 2015). However, if $S^{6+}/\Sigma S$ is buffered during sulfide fractionation by another multivalent element, conversion of S^{6+} to S^{2-} leads to a gradual increase in both melt $\delta^{34}S_{\Sigma S}$ and $\delta^{34}S_{S^{2-}}$ (Fig. 4b; Supplementary Information). This buffering effect means that the $\delta^{34}S$ values of moderately oxidized basalts that have fractionated sulfides, like those in Iceland, may be more positive than their mantle sources (Labidi et al. 2015).

The observed increase in $S^{6+}/\Sigma S$ below 6 wt.% MgO falls short of the modeled increase expected from sequestration of S^{2-} by sulfides (Fig. 2b), suggesting that at least some buffering of $S^{6+}/\Sigma S$ takes place in the melts. Iron may act as a redox buffer through the electron-exchange reaction (Fig. S5; Jugo et al. 2010).

$$S^{6+} + 8Fe^{2+} \rightleftharpoons S^{2-} + 8Fe^{3+} \tag{4}$$

In the Kverkfjöll samples, a subtle trend of increasing $\delta^{34}S_{S^{2-}}$ from –2.2 ‰ to –0.9 ‰ is observed during melt evolution between 7.5 to 4.0 wt.% MgO (Fig. 4b). A parallel $\delta^{34}S_{S^{2-}}$-versus MgO trend defined by the WRZ-ERZ-NRZ samples is offset to more positive $\delta^{34}S_{S^{2-}}$ values by ~0.5 ‰. The observed trends could be explained by redox buffering-induced $\delta^{34}S$ fractionation during sulfide melt formation. However, the large $\delta^{34}S$ variability in more primitive samples (MgO > 6 wt.%) cannot be explained by melt derivation from a homogenous mantle source, even if sulfide formation during Phase 1 is allowed (Fig. 4b). Instead, the data is most easily explained by primary melt variability of $\delta^{34}S_{S^{2-}}$ between approximately –2.5 and –0.1 ‰.

4.3. Sulfur heterogeneity in the Iceland mantle

Given that partial melting does not fractionate S isotopes, the $\delta^{34}S$, $\Delta^{33}S$ and $\Delta^{36}S$ values of mantle protoliths are passed on to primary mantle melts (Labidi and Cartigny 2016). While subsequent melt mixing in lower crustal or sub-Moho magma reservoirs may blunt the most extreme source signatures, bulk measurements of relatively primitive glasses are able to capture a major part of the existing mantle heterogeneity in Iceland (Shorttle and Maclennan

2011). Other types of crustal magmatic processing, such as sulfide immiscibility and crustal assimilation, are only expected to have a minor effect on the δ^{34}S signatures of primitive (MgO > 6 wt.%), undegassed samples (Sections 4.1 and 4.2). We consider the $\delta^{34}S_{S^{2-}}$ values of such samples to be representative of primary melt compositions within instrumental error. Degassed samples, and samples with MgO lower than 6 wt.% are filtered out in Figs. 6a, 7a and 8a. The Δ^{33}S values are not affected by either degassing, sulfide melt fractionation (Labidi et al. 2014) or $S^{6+}/\Sigma S$, so all Δ^{33}S glass analyses are thought to reflect source values and are plotted in Figs. 6-9. In Figs. 6a, 7a and 8a we plot the $\delta^{34}S_{\Sigma S}$ value that is calculated from the measured $S^{6+}/\Sigma S$ and $\delta^{34}S_{S^{2-}}$ values assuming isotopic equilibrium between sulfur species so that

$$\delta^{34}S_{\Sigma S} = S^{6+}/\Sigma S \times (\Delta^{34}S_{\mathrm{sulfate-sulfide}} + \delta^{34}S_{S^{2-}}) + (1 - S^{6+}/\Sigma S) \times \delta^{34}S_{S^{2-}} \qquad (5)$$

This adjustment is made in order to be able to compare our δ^{34}S data with published MORB data. MORBs are almost devoid of sulfate ($S^{6+}/\Sigma S \approx 0$; Labidi et al. 2014) so that $\delta^{34}S_{\Sigma S} \approx \delta^{34}S_{S^{2-}}$, whereas the Icelandic samples are more oxidized and their measured $\delta^{34}S_{S^{2-}}$ underestimate $\delta^{34}S_{\Sigma S}$ values by approximately 0.1-0.7 ‰.

4.3.1 Mantle sulfur isotopic signatures and relationship to other mantle source indicators

The large δ^{34}S variability identified in the Iceland mantle ($\delta^{34}S_{S^{2-}} = -2.5$ to -0.1 ‰, or equivalently, $\delta^{34}S_{\Sigma S} = -1.8$ to $+0.5$ ‰) exceeds that of unaltered MORBs and points to mantle heterogeneity with respect to sulfur (Figs. 4, 6-8). If sulfur shares a common history with known Icelandic mantle components, a correlation is expected between δ^{34}S-Δ^{33}S and traditional tracers of mantle heterogeneity, such as Nb/Zr, ^{3}He/^{4}He and ^{206}Pb/^{204}Pb.

The three most depleted samples (Nb/Zr < 0.05) show the greatest variation in $\delta^{34}S_{\Sigma S}$ values, representing the full of range of Icelandic mantle values of -1.8 to $+0.5$ ‰ (Fig. 6a). Similar, but slightly smaller $\delta^{34}S_{\Sigma S}$ variation of -1.8 to 0.0 ‰ is found in the most enriched samples (Nb/Zr > 0.10). Whereas enriched trace element signatures in Iceland are tied to enriched radiogenic isotope signatures (Shorttle and Maclennan 2011), the apparent lack of correlation of Nb/Zr with δ^{34}S or Δ^{33}S (Fig. 6) indicates that sulfur is partly decoupled from the lithophile, non-volatile elements and their isotopes. However, δ^{34}S-Δ^{33}S signatures can be tied to Icelandic mantle components using available ^{206}Pb/^{204}Pb (Fig. 7) and ^{3}He/^{4}He (Fig. 8) data, which have been used to demarcate primordial, recycled, and local DMM components in the Iceland plume (e.g., Hanan et al. 2000, Füri et al. 2010). Four mantle components are required to explain the combined $^{3}He/^{4}He$-$\delta^{34}S$-$\Delta^{33}S$-$^{206}Pb/^{204}Pb$ systematics:

(1) Local DMM contributes a low-$^{3}He/^{4}He$ (8±1 R_A) Icelandic end-member with typical MORB-like $\delta^{34}S_{\Sigma S}$ = -1.3 ‰ and $\Delta^{33}S$ = 0 ‰. The samples closest to the DMM component come from the NRZ (cf. Hanan et al. 2000).

(2) Plume 1 component has non-radiogenic $^{206}Pb/^{204}Pb$ (18.2-18.5) and is tied to one of the highest modern $^{3}He/^{4}He$ of 33.6 R_A measured in present-day hotspots (Jackson et al. 2020), representing a primordial mantle component. This component has DMM-like $\Delta^{33}S$ of 0 ‰ but a higher $\delta^{34}S_{\Sigma S}$ value of ~0 ‰. Plume 1 is expressed most clearly by the ERZ basalts in central Iceland, close to the suggested center of the plume (Rasmussen et al. 2020).

(3) Plume 2 is a second Icelandic high-$^{3}He/^{4}He$ component (up to 25.7 R_A) marked by radiogenic $^{206}Pb/^{204}Pb$ (19.1-19.3) (Mundl-Petermeier et al. 2019, Jackson et al. 2020). It is exclusively sampled by the propagating rift volcanoes in the SIVZ, which have an average $\Delta^{33}S$ value of 0.004±0.005 ‰. The $\delta^{34}S_{\Sigma S}$ of Plume 2 is assumed to be –1.2 ‰ based on the most primitive SIVZ sample THRI-2. Plume 2 component is thought to represent intermingling of primordial mantle with recycled oceanic crust (Rasmussen et al. 2020). This proposed origin of Plume 2 component is consistent with its DMM-like $\delta^{34}S_{\Sigma S}$-$\Delta^{33}S$ signature, as the $\delta^{34}S$ of oceanic lithosphere is approximately preserved during subduction to the deep mantle (Alt 1995; Li et al. 2020).

(4) To explain the low-$\delta^{34}S$ trend defined by Kverkfjöll lavas (Section 4.2; Fig. 4b) and the tendency of Iceland lavas toward negative $\Delta^{33}S$ signatures compared to DMM (Fig. 5), we propose a previously unrecognized Icelandic mantle component – Enriched Mantle Wedge (EMW). Based on the $^{3}He/^{4}He$-$\delta^{34}S$-$\Delta^{33}S$ systematics (Fig. 8), EMW is assigned negative $\delta^{34}S_{\Sigma S}$ and $\Delta^{33}S$ values of –2.5 ‰ and –0.040 %, respectively, and a DMM-like $^{3}He/^{4}He$ of 8 R_A. EMW is sampled most clearly by Kverkfjöll lavas, but its influence is seen across lavas from all rift zones as negatively trending $\delta^{34}S_{\Sigma S}$ and $\Delta^{33}S$ values with decreasing $^{3}He/^{4}He$ (Fig. 8). The three lowest-$\delta^{34}S$ samples (MID-1, NAL-356, NAL-585) all have similar $^{206}Pb/^{204}Pb$ of ~18.5, which is taken as the signature of EMW. The SNVZ basalts also have MORB-like $^{3}He/^{4}He$ and the lowest $\Delta^{33}S$ (down to –0.035 ‰) in Iceland, suggesting contributions from the EMW component (Fig. 8b). However, as the SNVZ samples are evolved and highly degassed, their source $\delta^{34}S$ signature cannot be inferred.

4.3.2 Origin of recycled sulfur in the Iceland mantle

Previous observations of non-zero $\Delta^{33}S$ values in OIBs from Mangaia (Cabral et al. 2014; Dottin et al. 2020b) and Pitcairn (Delavault et al. 2016) provide evidence for the resurgence of deep recycled Archaean sediments – the only known major terrestrial reservoir with S-MIF signatures ($\Delta^{33}S$ between –2.5 and 11.5 ‰; Johnston 2011). The large negative $\Delta^{33}S$ anomalies at Pitcairn and Mangaia are coupled to highly negative $\delta^{34}S$ (Cabral et al. 2014, Delavault et al. 2016). Subducted sediments are also thought to form a positive $\delta^{34}S$ end-member in the MORB source mantle (Labidi et al. 2013, 2014), the Samoan EM2 component (Labidi et al. 2015), as well as the Canary Islands HIMU component (Beaudry et al. 2018), which all lack resolvable $\Delta^{33}S$ anomalies.

Negative $\Delta^{33}S$ and $\delta^{34}S$ values in Icelandic basalts are tied to a mantle component with MORB-like $^{3}He/^{4}He$ and $^{206}Pb/^{204}Pb$ (Figs. 7 and 8), but also elevated Ba/La (Fig. S8). These characteristics are compatible with subduction fluid-enriched mantle wedge (EMW) type component, i.e., a DMM-like component that has been enriched with sediment-derived fluids from a subducting plate (cf. Richter et al. 2020). Influx of subduction-related volatiles to the upper mantle from subducting slabs is thought to contribute to the volatile heterogeneity of MORB sources (Dixon et al. 2017), including the North Atlantic mantle, as well as Iceland (Halldórsson et al. 2016b; Hauri et al. 2018, Richter et al. 2020). As ambient DMM constitutes a geochemical endmember in Icelandic basalts (Hanan et al. 2000), it is worthwhile to entertain the possibility that the EMW component represents a local upper mantle anomaly resulting from shallow subduction-fluid metasomatism, rather than a deep-sourced plume component.

Plausible past subduction events in the region that could have produced the EMW component include Palaeozoic subduction episodes that lead to the closure of the proto-Atlantic Iapetus ocean (Halldórsson et al. 2016b; Hauri et al. 2018) and the Early Cretaceous South Anuyi subduction event (145-120 Ma; Richter et al. 2020).

Subduction fluids are potent agents of mantle metasomatism, and may transport 6-20 % of the S budget of the slab to the the mantle wedge region at 30-230 km depth (Jégo and Dasgupta 2013; Li et al. 2020). Fluids equilibrated with subducting metasediments at ~100 km depth have highly negative $\delta^{34}S$ values of down to -8 ‰ and high sulfur concentrations of ~1 wt.% (Li et al. 2020). Sediment-derived fluids could also acquire measurable negative $\Delta^{33}S$ signatures through even minor incorporation of Archaean sediments derived from continental margins adjacent to the subduction zone. Thus, subduction fluid metasomatism could potentially lead to lowered $\delta^{34}S$ and $\Delta^{33}S$ of the mantle wedge. The EMW component can be created by an admixture of DMM, and ~0.5 wt.% of metasediment-derived subduction fluid with moderately negative δ^{34}S and Δ^{33}S signatures of –5 ‰ and –0.130 ‰, respectively (Fig. 8).

Subduction fluids are also enriched in fluid-mobile elements like Ba, leading to elevated Ba/La in arc and back-arc basin basalts and mantle wedges (Leeman et al. 1994). A negative correlation is observed between Ba/La and ^{3}He/^{4}He in Icelandic basalts (Fig. S8), supporting the presence of an Icelandic mantle component that resembles subduction fluid-enriched DMM. For example, the Kverkfjöll and SNVZ samples that have the lowest ^{3}He/^{4}He, δ^{34}S and Δ^{33}S values in Iceland, also have highest Ba/La (10.4-12.4). A fluid-enriched source for the SNVZ basalts is also suggested by their elevated W concentrations (Mundl-Petermeier et al. 2019).

As opposed to a deep-sourced plume component, we propose that EMW represents a shallow low-δ^{34}S-Δ^{33}S mantle anomaly in the North Atlantic upper mantle, created during past subduction events in the region, that has become captured *en passant* by the upwelling Iceland mantle plume.

4.4 Implications for the origin of sulfur in the primordial mantle

Assuming that the association of high-^{3}He/^{4}He Iceland samples with ^{129}Xe anomalies and negative μ^{182}W (where μ^{182}W represents deviations of the modern upper mantle ^{182}W/^{184}W in ppm) is indicative of an early-Hadean origin (>4.45 Ga; Mukhopadhyay 2012; Mundl-Petermeier et al. 2019), the formation of the high-^{3}He/^{4}He mantle domain predates the oldest surviving terrestrial crust (Jack Hill zircons, up to 4.40 Ga; Wilde et al. 2001) and the peak of late accretion at 4.2-4.0 Ga (Bottke and Norman 2017). This primordial mantle domain is associated spatially with ultra-low seismic wave velocity zones (ULVZs) identified at the base of the mantle at the roots of the high-^{3}He/^{4}He plumes Hawaii, Iceland and Samoa (Yuan and Romanowicz 2017 and references therein). The hot, potentially partly molten state of ULVZs could promote transport of elements, including S, across the core-mantle boundary (Rizo et al. 2019, Mundl-Petermeier et al. 2020). Thus, the sulfur isotopic fingerprint of the high-^{3}He/^{4}He mantle has the potential to constrain key questions remaining about Early Earth processes, as well as the nature and extent of core-mantle interaction (e.g., Mundl-Petermeier et al. 2020).

Our access to undegassed subglacial glass samples allows us to make the first estimate of the $\delta^{34}S_{\Sigma S}$ signature of the high-^{3}He/^{4}He mantle. Icelandic basalts show increasing

$\delta^{34}S_{\Sigma S}$ values with increasing $^3He/^4He$, projecting toward a primordial plume component with a near-chondritic $\delta^{34}S_{\Sigma S}$ value of ~0 ‰ (Plume 1 in Fig. 8a). This chondritic $\delta^{34}S_{\Sigma S}$ signature contrasts with the distinctly negative, non-chondritic $\delta^{34}S_{\Sigma S}$ signature of the DMM (-1.28±0.33 ‰; Labidi et al. 2013) and poses the question of why they are different.

The negative $\delta^{34}S_{\Sigma S}$ signature of DMM has been explained to result from core-mantle segregation, because the metallic iron alloy that forms the core is enriched in ^{34}S during metal-silicate equilibration (i.e., $\varepsilon^{34}S_{metal\text{-}silicate} > 0$; Labidi et al., 2013, 2016, Labidi and Cartigny 2016). Depletions of highly siderophile elements (HSEs) in high-$^3He/^4He$ lavas relative to chondrites indicate that the high-$^3He/^4He$ mantle domain experienced core extraction (Mundl et al. 2017, 2020), similarly to MORBs. If we accept the Labidi and Cartigny (2016) model, the high-$^3He/^4He$ mantle would be expected to have a non-chondritic and negative $\delta^{34}S_{\Sigma S}$ signature. Thus, the contrasting $\delta^{34}S_{\Sigma S}$ signatures of DMM and the high-$^3He/^4He$ mantle present an apparent paradox. Below, we discuss mechanisms that could affect the S isotopic composition of the two mantle reservoirs differently.

First, it is conceivable that sulfur was extracted from the high-$^3He/^4He$ mantle during core formation at conditions where $^{34}S/^{32}S$ fractionation is negligible. If the high-$^3He/^4He$ mantle equilibrated with a metallic iron alloy at higher temperature compared to the DMM, the accompanying $\varepsilon^{34}S_{metal\text{-}silicate}$ fractionation factor could be considerably smaller. However, extrapolation of $\varepsilon^{34}S_{metal\text{-}silicate}$ from experimental conditions (up to 1.5 GPa and 1650 °C; Labidi et al. 2016) to lower mantle conditions (up to 136 GPa and ~4000 K at the core-mantle boundary at present) is difficult because of the opposing effects of increasing T (decreases $^{34}S/^{32}S$ fractionation) and P (increases $^{34}S/^{32}S$ fractionation; Labidi and Cartigny 2016). Alternatively, rather than resulting from metal/silicate equilibrium, it is possible that the S isotopic signature of the high-$^3He/^4He$ mantle is controlled by equilibrium with a sulfide liquid phase ("Hadean matte"; O'Neill 1991) which is associated with negligible $^{34}S/^{32}S$ fractionation (Labidi and Cartigny 2016). Although the fraction of S in the mantle affected by sulfide-silicate equilibrium is estimated to be less than ~10% (Labidi and Cartigny 2016), the high-$^3He/^4He$ mantle could be disproportionally affected compared to the DMM due to its location at the base of the mantle, where a 2-35 km layer of sulfide liquid is thought to have ponded at the late stage of core-mantle differentiation (Savage et al. 2015). Either of these scenarios could potentially explain the contrasting $\delta^{34}S_{\Sigma S}$ signatures of the high-$^3He/^4He$ mantle and the DMM by only invoking core extraction from the silicate mantle.

Second, the S isotopic composition of the high-$^3He/^4He$ mantle could be influenced by core-mantle exchange through similar mechanisms that have been recently suggested to explain negative $\mu^{182}W$ anomalies present in high-$^3He/^4He$ lavas (Mundl et al. 2017, Mundl-Petermeier et al. 2020, Jackson et al. 2020). Combined $^3He/^4He$-$\Delta^{33}S$-$\mu^{182}W$ data from Iceland and Samoa – the only high-$^3He/^4He$ locations where coupled data are available – show that Samoan and Icelandic basalts converge toward near-0 $\Delta^{33}S$ values with increasing $^3He/^4He$ (Fig. 8b) and decreasing $\mu^{182}W$ (Fig. 9). The chondritic $\Delta^{33}S$ signature of high-$^3He/^4He$ lavas corroborates the suggestion that they sample a primordial mantle *least* modified by subducted crustal materials (Jackson et al. 2020). The coupled $^3He/^4He$-$\delta^{34}S$ (Fig. 8a) and $^3He/^4He$-$\Delta^{33}S$-$\mu^{182}W$ (Figs. 8b and 9) systematics suggest that the near-chondritic $\delta^{34}S_{\Sigma S}$ is linked to negative $\mu^{182}W$. Therefore, it is important to explore whether a single process could explain the $\delta^{34}S_{\Sigma S}$-$\Delta^{33}S$-$\mu^{182}W$ signature of the high-$^3He/^4He$ mantle.

The main current hypothesis to explain the negative correlation between $\mu^{182}W$ and $^3He/^4He$ in OIBs is to incorporate W from the core, which is inferred to have very low $\mu^{182}W$ (-220 ppm) and high W concentration (~500 ppb) (Mundl-Petermeier et al., 2019, 2020; Rizo et al. 2019). The core is also the main reservoir of Earth's sulfur, with a 100-fold higher S content relative to the mantle (approximately 2 wt.% and 200 ppm, respectively) and an assumed chondritic $\Delta^{33}S$-$\delta^{34}S$ signature (Labidi et al. 2013). Thus, incorporation of small amounts of core material could simultaneously explain both the negative $\mu^{182}W$ and the chondritic $\delta^{34}S$ signature of the high $^3He/^4He$ mantle. However, because OIBs are not enriched in highly siderophile elements (HSEs), input of bulk core metal in plume sources is considered unlikely (Mundl-Petermeier 2020). Instead, Mundl-Petermeier et al. (2020) hypothesized that equilibration of the metallic outer core and a basal layer of a primordial magma ocean could produce a remnant lower mantle reservoir with core-like $\mu^{182}W$ signature without elevated HSE abundances. However, if the the $\varepsilon^{34}S_{\text{metal-silicate}}$ fractionation factor remains positive at lower mantle P-T-conditions (Labidi et al. 2016), applied to S, the core-mantle equilibration model of Mund-Petermeier et al. (2020) would generate (or maintain) a negative $\delta^{34}S_{\Sigma S}$ signature for the high-$^3He/^4He$ mantle, failing to explain its chondritic $\delta^{34}S_{\Sigma S}$ signature.

As an alternative process of adding negative $\mu^{182}W$ core material to the lower mantle, Rizo et al. (2019) showed that Si-Mg-Fe oxides that exsolve from the outer core preferentially incorporate W over HSEs. These oxides are buoyant and would accumulate at the core-mantle boundary, potentially contributing to the selective transport of core-derived W to the lower mantle. It is conceivable that S with chondritic isotopic composition could be transported to the lower mantle through this or a similar process. However, an extension of either of the two models to account for a chondritic S isotopic composition of the high-

^{3}He/^{4}He mantle remains highly hypothetical at present, as key parameters, such as partitioning of S to Si-Mg-Fe oxides and the $\varepsilon^{34}S_{\text{metal-silicate}}$ fractionation factor at high P and T, remain poorly constrained.

Although many open questions remain, the near-chondritic S isotopic composition of the high-^{3}He/^{4}He mantle provides a new important constraint for future models on the nature and extent of chemical interactions between the core and the mantle during early planetary differentiation, as well as in the present.

5 CONCLUSIONS

This study presents S concentration, speciation ($S^{6+}/\Sigma S$) and isotope data acquired from 62 samples covering the main neovolcanic zones of Iceland. Focusing on undegassed, subglacial basaltic glasses, the data provide a unique window to the sulfur isotopic evolution of OIB magmas, constraining the $\delta^{34}S$-$\Delta^{33}S$ signatures of various Icelandic mantle components. Undegassed Icelandic glasses contain between 300 and 1570 ppm sulfur and are mildly oxidized ($S^{6+}/\Sigma S = 0.05–0.20$). Melts reach sulfide saturation at MgO ≈ 6 wt.%, which leads to S and Cu depletions concurrent with increasing $S^{6+}/\Sigma S$ and $\delta^{34}S_{S^{2-}}$ during subsequent melt evolution. The observed $\delta^{34}S_{S^{2-}}$ (–2.5 to -0.1‰) and $\Delta^{33}S$ (–0.035 to +0.011 ‰) variability expressed by primitive Icelandic basalts exceeds that measured in MORBs. We infer an Icelandic mantle component with negative $\delta^{34}S_{\Sigma S} = –2.5$ wt.% and negative $\Delta^{33}S = –0.40$ ‰ that is associated with MORB-like ^{3}He/^{4}He (8 R_A) and elevated Ba/La (>12). We suggest that this mantle component (EMW) represents subduction fluid-enriched mantle wedge-type material present in the local upper mantle, that became entrained in the Iceland plume *en route* to the surface. High-^{3}He/^{4}He and low-μ^{182}W samples from NRZ and ERZ converge toward $\Delta^{33}S$ and $\delta^{34}S_{\Sigma S}$ values of 0 ‰. The near-chondritic $\delta^{34}S_{\Sigma S}$ signature inferred for the primordial high-^{3}He/^{4}He reservoir is difficult to reconcile with the sub-chondritic $\delta^{34}S_{\Sigma S}$ signature of DMM, and may suggest that the two mantle domains experienced core extractions at different conditions during planetary differentiation, or alternatively, points toward a previously unidentified flux of S from the core to the high-^{3}He/^{4}He reservoir.

ACKNOWLEDGEMENTS

This study has been supported by NordVulk fellowships awarded to ER and JGR, as well as a University of Iceland Research Fund Doctoral grant awarded to ER. SAH acknowledges support from the Icelandic Research Fund (Grant #196139-051) and the University of Iceland Research Fund. GI acknowledges the financial support of the Simons Foundation under the auspices of the SCOL incentive awarded to Roger Summons at MIT. William Olszewski's reliable help with the SF$_6$ GC-IRMS line at MIT is thankfully acknowledged. Hugh O'Brien at GTK was of great help during trace element analysis of the KVK samples. Simon Matthews and Maja Bar Rasmussen are thanked for commenting on early versions of the manuscript.

REFERENCES

Alt, J. C. (1995) Sulfur isotopic profile through the oceanic crust: sulfur mobility and seawater-crustal sulfur exchange during hydrothermal alteration. *Geology*, *23*, 585–588.

Ariskin, A. A., Bychkov, K. A., Nikolaev, G. S., & Barmina, G. S. (2018). The Comagmat-5: modeling the effect of Fe–Ni sulfide immiscibility in crystallizing magmas and cumulates. *Journal of Petrology*, *59*(2), 283-298.

Beaudry, P., Longpré, M. A., Economos, R., Wing, B. A., Bui, T. H., & Stix, J. (2018). Degassing-induced fractionation of multiple sulphur isotopes unveils post-Archaean recycled oceanic crust signal in hotspot lava. *Nature communications*, *9*(1), 1-12.

Bézos, A., Lorand, J. P., Humler, E., & Gros, M. (2005). Platinum-group element systematics in Mid-Oceanic Ridge basaltic glasses from the Pacific, Atlantic, and Indian Oceans. *Geochimica et Cosmochimica Acta*, *69*(10), 2613-2627.

Bottke, W. F., & Norman, M. D. (2017). The late heavy bombardment. *Annual Review of Earth and Planetary Sciences*, *45*.

Cabral, R. A., Jackson, M. G., Rose-Koga, E. F., Koga, K. T., Whitehouse, M. J., Antonelli, M. A., Farquhar, J., Day, J.M.D., & Hauri, E. H. (2013). Anomalous sulphur isotopes in plume lavas reveal deep mantle storage of Archaean crust. *Nature*, *496*(7446), 490-493.

Coplen, T. B., & Krouse, H. R. (1998). Sulphur isotope data consistency improved. *Nature*, *392*(6671), 32-32.

Delavault, H., Chauvel, C., Thomassot, E., Devey, C. W., & Dazas, B. (2016). Sulfur and lead isotopic evidence of relic Archean sediments in the Pitcairn mantle plume. *Proceedings of the National Academy of Sciences*, *113*(46), 12952-12956.

Ding, S., & Dasgupta, R. (2018). Sulfur inventory of ocean island basalt source regions constrained by modeling the fate of sulfide during decompression melting of a heterogeneous mantle. *Journal of Petrology*, *59*(7), 1281-1308.

Dixon, J. E., Bindeman, I. N., Kingsley, R. H., Simons, K. K., Le Roux, P. J., Hajewski, T. R., Swart, P., Langmuir, C.H., Ryan, J.G., Walowski, K.J., Wada, I., & Wallace, P. J. (2017). Light stable isotopic compositions of enriched mantle sources: Resolving the dehydration paradox. *Geochemistry, Geophysics, Geosystems*, *18*(11), 3801-3839.

Dottin III, J. W., Labidi, J., Lekic, V., Jackson, M. G., & Farquhar, J. (2020a). Sulfur isotope characterization of primordial and recycled sources feeding the Samoan mantle plume. *Earth and Planetary Science Letters*, *534*, 116073.

Dottin III, J. W., Labidi, J., Jackson, M. G., Woodhead, J., & Farquhar, J. (2020b) Isotopic evidence for multiple recycled sulfur reservoirs in the Mangaia mantle plume. *Geochemistry, Geophysics, Geosystems*, e2020GC009081.

Gunnarsson-Robin, J., Stefánsson, A., Ono, S., & Torssander, P. (2017). Sulfur isotopes in Icelandic thermal fluids. *Journal of Volcanology and Geothermal Research*, *346*, 161-179.

Halldórsson, S. A., Barnes, J. D., Stefánsson, A., Hilton, D. R., Hauri, E. H., & Marshall, E. W. (2016a). Subducted lithosphere controls halogen enrichments in the Iceland mantle plume source. *Geology*, *44*(8), 679-682.

Halldórsson, S. A., Hilton, D. R., Barry, P. H., Füri, E., & Grönvold, K. (2016b). Recycling of crustal material by the Iceland mantle plume: New evidence from nitrogen elemental and isotope systematics of subglacial basalts. *Geochimica et Cosmochimica Acta*, *176*, 206-226.

Halldórsson, S. A., Bali, E., Hartley, M. E., Neave, D. A., Peate, D. W., Guðfinnsson, G. H., Bindeman, I., Whitehouse, M.J., Riishuus, M.S., Pedersen, G.B.M., Jakobsson, S., Askew, R., Gallagher, C.R., Guðmundsdóttir, E.R., Gudnason, J., Moreland, W.M., Óskarsson, B.V., Nikkola, P., Reynolds, H.I., Schmith, H., & Thordarson, T. (2018). Petrology and geochemistry of the 2014–2015 Holuhraun eruption, central Iceland: compositional and mineralogical characteristics, temporal variability and magma storage. *Contributions to Mineralogy and Petrology*, *173*(8), 64.

Hanan, B. B., Blichert-Toft, J., Kingsley, R., & Schilling, J. G. (2000). Depleted Iceland mantle plume geochemical signature: Artifact of multicomponent mixing?. *Geochemistry, Geophysics, Geosystems*, *1*(4).

Harðardóttir, S., Halldórsson, S. A., & Hilton, D. R. (2018). Spatial distribution of helium isotopes in Icelandic geothermal fluids and volcanic materials with implications for location, upwelling and evolution of the Icelandic mantle plume. *Chemical Geology*, *480*, 12-27.

Hauri, E. H., Maclennan, J., McKenzie, D., Gronvold, K., Oskarsson, N., & Shimizu, N. (2018). CO2 content beneath northern Iceland and the variability of mantle carbon. *Geology*, *46*(1), 55-58.

Jackson, M. G., Blichert-Toft, J., Halldórsson, S.A., Mundl-Petermeier, A., Bizimis, M., Kurz, M.D., Price, A.A., Harðardóttir, S. , Willhite, L.N.,. Breddam, K., Becker, T.W., Fischer, R.A. (2020) Ancient helium and tungsten isotopic signatures preserved in mantle domains least modified by crustal recycling. *Proceedings of the National Academy of Sciences*, *117*(49), 30993-31001.

Jégo, S. & Dasgupta, R (2013). Fluid-present melting of sulfide-bearing ocean-crust: experimental constraints on the transport of sulfur from subducting slab to mantle wedge. *Geochimica et Cosmochimica Acta*, *110*, 106–134.

Jenner, F. E., O'Neill, H. S. C., Arculus, R. J., & Mavrogenes, J. A. (2010). The magnetite crisis in the evolution of arc-related magmas and the initial concentration of Au, Ag and Cu. *Journal of Petrology*, *51*(12), 2445-2464.

Johnston, D. T. (2011). Multiple sulfur isotopes and the evolution of Earth's surface sulfur cycle. *Earth-Science Reviews*, *106*(1-2), 161-183.

Jugo, P.J., Wilke, M., & Botcharnikov, R.E. (2010). Sulfur K-edge XANES analysis of natu- ral and synthetic basaltic glasses: implications for S speciation and S content as function of oxygen fugacity. *Geochimica et Cosmochimica Acta*, *74*(20), 5926–5938.

Labidi, J., Cartigny, P., Birck, J. L., Assayag, N., & Bourrand, J. J. (2012). Determination of multiple sulfur isotopes in glasses: A reappraisal of the MORB δ34S. *Chemical Geology*, *334*, 189-198.

Labidi, J., Cartigny, P., & Moreira, M. (2013). Non-chondritic sulphur isotope composition of the terrestrial mantle. *Nature*, *501*(7466), 208-211.

Labidi, J., Cartigny, P., Hamelin, C., Moreira, M., & Dosso, L. (2014). Sulfur isotope budget (32S, 33S, 34S and 36S) in Pacific–Antarctic ridge basalts: A record of mantle source heterogeneity and hydrothermal sulfide assimilation. *Geochimica et Cosmochimica Acta*, *133*, 47-67.

Labidi, J., Cartigny, P., & Jackson, M. G. (2015). Multiple sulfur isotope composition of oxidized Samoan melts and the implications of a sulfur isotope 'mantle array' in chemical geodynamics. *Earth and Planetary Science Letters*, *417*, 28-39.

Labidi, J., & Cartigny, P. (2016). Negligible sulfur isotope fractionation during partial melting: Evidence from Garrett transform fault basalts, implications for the late-veneer and the hadean matte. *Earth and Planetary Science Letters*, *451*, 196-207.

Labidi, J., Shahar, A., Le Losq, C., Hillgren, V. J., Mysen, B. O., & Farquhar, J. (2016). Experimentally determined sulfur isotope fractionation between metal and silicate and implications for planetary differentiation. *Geochimica et Cosmochimica Acta*, *175*, 181-194.

Lee, C. T. A., Luffi, P., Chin, E. J., Bouchet, R., Dasgupta, R., Morton, D. M., Le Roux, V., Yin, Q., & Jin, D. (2012). Copper systematics in arc magmas and implications for crust-mantle differentiation. *Science, 336*(6077), 64-68

Leeman, W. P., Carr, M. J., & Morris, J. D. (1994). Boron geochemistry of the Central American volcanic arc: constraints on the genesis of subduction-related magmas. *Geochimica et Cosmochimica Acta*, *58*(1), 149-168.

Li, J. L., Schwarzenbach, E. M., John, T., Ague, J. J., Huang, F., Gao, J., Klemd, R., Whitehouse, M., & Wang, X. S. (2020). Uncovering and quantifying the subduction zone sulfur cycle from the slab perspective. *Nature Communications*, *11*(1), 1-12.

Macpherson, C. G., Hilton, D. R., Day, J. M., Lowry, D., & Grönvold, K. (2005). High-^{3}He/^{4}He, depleted mantle and low-δ^{18}O, recycled oceanic lithosphere in the source of central Iceland magmatism. *Earth and Planetary Science Letters*, *233*(3-4), 411-427.

Mukhopadhyay, S. (2012). Early differentiation and volatile accretion recorded in deep-mantle neon and xenon. *Nature*, *486*(7401), 101-104.

Mundl, A., Touboul, M., Jackson, M. G., Day, J. M., Kurz, M. D., Lekic, V., Helz, R.T., & Walker, R. J. (2017). Tungsten-182 heterogeneity in modern ocean island basalts. *Science*, *356*(6333), 66-69.

Mundl-Petermeier, A., Walker, R. J., Jackson, M. G., Blichert-Toft, J., Kurz, M. D., & Halldórsson, S. A. (2019). Temporal evolution of primordial tungsten-182 and ^{3}He/^{4}He signatures in the Iceland mantle plume. *Chemical Geology*, *525*, 245-259.

Mundl-Petermeier, A., Walker, R. J., Fischer, R. A., Lekic, V., Jackson, M. G., & Kurz, M. D. (2020). Anomalous 182W in high 3He/4He ocean island basalts: Fingerprints of Earth's core? *Geochimica et Cosmochimica Acta*, *271*, 194-211.

Ono, S., Wing, B., Rumble, D., & Farquhar, J. (2006). High precision analysis of all four stable isotopes of sulfur (^{32}S, ^{33}S, ^{34}S and ^{36}S) at nanomole levels using a laser fluorination isotope-ratio-monitoring gas chromatography–mass spectrometry. *Chemical Geology*, *225*(1-2), 30-39.

Ono, S., Keller, N. S., Rouxel, O., & Alt, J. C. (2012). Sulfur-33 constraints on the origin of secondary pyrite in altered oceanic basement. *Geochimica et Cosmochimica Acta*, *87*, 323-340.

Ranta, E., Barnes, J.D., Halldórsson, S.A., Jónasson, K., Stefánsson A. (2021). Chlorine isotope ratios record magmatic brine assimilation during rhyolite genesis. *Geochemical Perspectives Letters*, *16*, 35-39.

Rasmussen, M. B., Halldórsson, S. A., Gibson, S. A., & Guðfinnsson, G. H. (2020). Olivine chemistry reveals compositional source heterogeneities within a tilted mantle plume beneath Iceland. *Earth and Planetary Science Letters*, *531*, 116008.

Reekie, C. D. J., Jenner, F. E., Smythe, D. J., Hauri, E. H., Bullock, E. S., & Williams, H. M. (2019). Sulfide resorption during crustal ascent and degassing of oceanic plateau basalts. *Nature communications*, *10*(1), 1-11.

Richter, M., Nebel, O., Maas, R., Mather, B., Nebel-Jacobsen, Y., Capitanio, F. A., Dick, H.J.B., & Cawood, P. A. (2020). An Early Cretaceous subduction-modified mantle underneath the ultraslow spreading Gakkel Ridge, Arctic Ocean. *Science advances*, *6*(44), eabb4340.

Rizo, H., Andrault, D., Bennett, N. R., Humayun, M., Brandon, A., Vlastélic, I., Moine, B., Poirier, A., Bouhifd, M.A. & Murphy, D. T. (2019). ^{182}W evidence for core-mantle interaction in the source of mantle plumes. *Geochem. Perspect. Lett.*, *11*, 6-11.

Shorttle, O., & Maclennan, J. (2011). Compositional trends of Icelandic basalts: Implications for short–length scale lithological heterogeneity in mantle plumes. *Geochemistry, Geophysics, Geosystems*, *12*(11).

Torssander, P. (1989). Sulfur isotope ratios of Icelandic rocks. *Contributions to Mineralogy and Petrology*, *102*(1), 18-23.

Wallace, P. J., & Edmonds, M. (2011). The sulfur budget in magmas: evidence from melt inclusions, submarine glasses, and volcanic gas emissions. *Reviews in Mineralogy and Geochemistry*, *73*(1), 215-246.

Wieser, P. E., Jenner, F., Edmonds, M., Maclennan, J., & Kunz, B. E. (2020). Chalcophile elements track the fate of sulfur at Kīlauea Volcano, Hawai'i. *Geochimica et Cosmochimica Acta*, *282*, 245-275.

Wilde, S. A., Valley, J. W., Peck, W. H., & Graham, C. M. (2001). Evidence from detrital zircons for the existence of continental crust and oceans on the Earth 4.4 Gyr ago. *Nature*, *409*(6817), 175-178.

Yuan K. & Romanowicz B. (2017) Seismic evidence for partial melting at the root of major hot spot plumes. *Science* 357, 393.

FIGURES

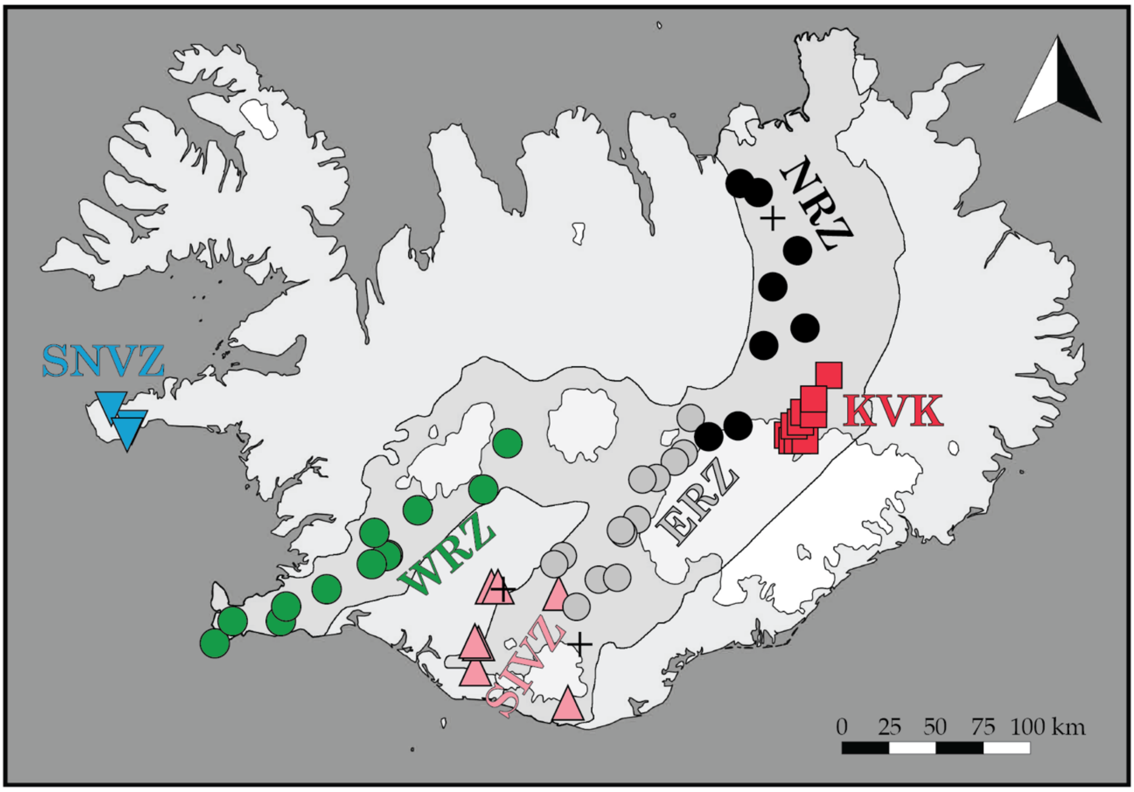

Figure 1 Map of Iceland showing sample locations of 59 subglacial pillow rim glass (circles, squares, triangles) and 3 subaerial lava samples (black crosses) analyzed in this study. The grey shaded area depicts presently active rift zones and the SIVZ propagating rift. Symbol types and colors used here to discriminate samples from different volcanic regions are maintained in all figures. Abbreviations: ERZ = Eastern Rift Zone, KVK = Kverkfjöll volcanic system, NRZ = Northern Rift Zone, SIVZ = South Iceland Volcanic Zone, SNVZ = Snæfellsnes Volcanic Zone, WRZ = Western Rift Zone and Reykjanes Peninsula.

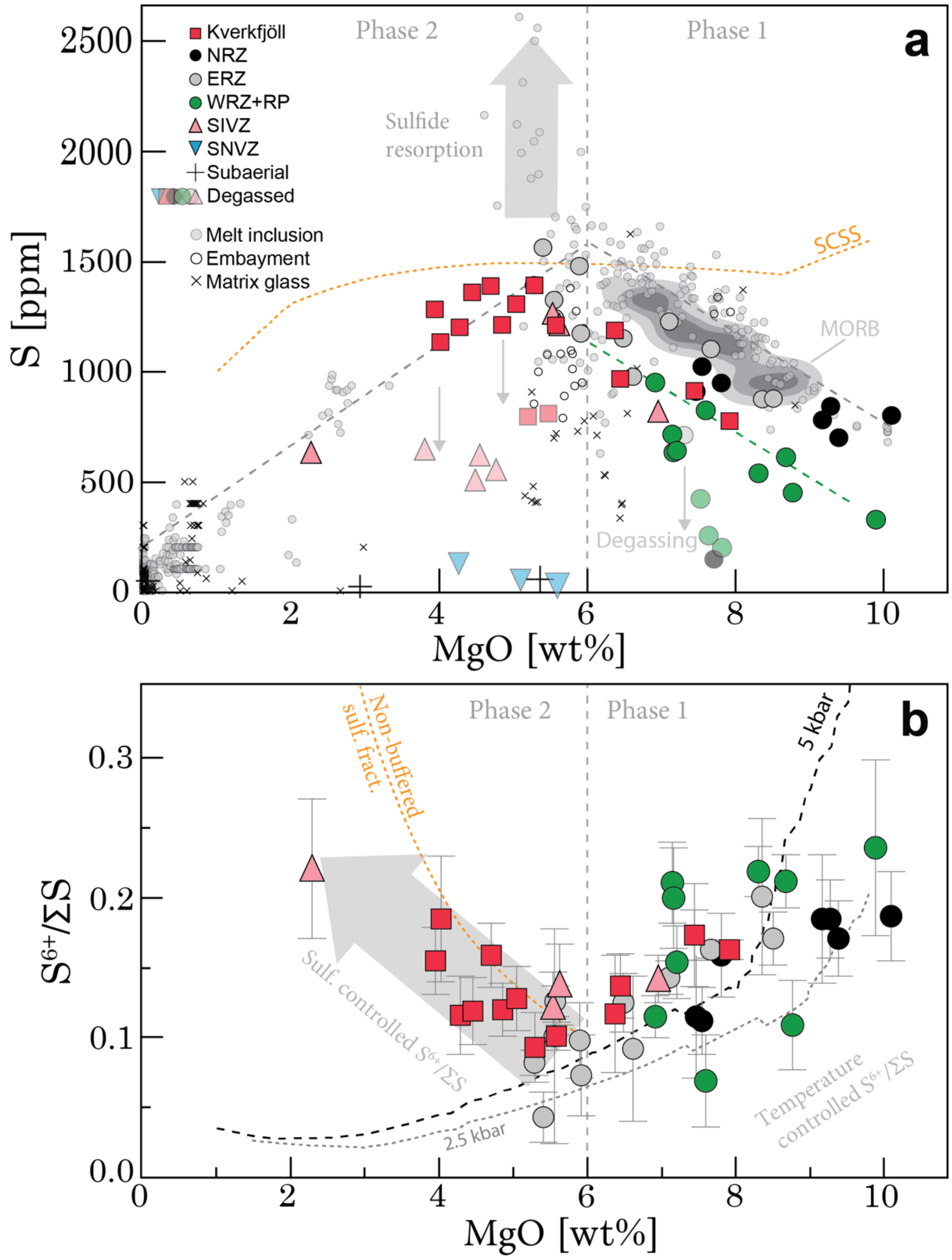

Figure 2 (a) Sulfur abundance versus MgO. Data from this study are superimposed on published melt inclusion data from Iceland (compilation from Ranta et al. 2021). The melt inclusion data define an undegassed S evolution trend (dashed grey lines) with an inflection point at MgO ≈ 6 wt.%, separating two distinct phases of melt evolution. In Phase 1, the WRZ basalts define a parallel, lower-S trend, indicated by the green dashed line. Samples deemed to have lost a significant amount of S by degassing are shown as transparent symbols (Supplementary Information). **(b)** Sulfur speciation versus MgO. Only undegassed samples are plotted (the full dataset is plotted in Fig. S3). Above MgO > 6 wt.%, decreasing $S^{6+}/\Sigma S$ during fractional crystallization is controlled by temperature (Supplementary Information). Below 6 wt.% MgO, sulfide precipitation causes an increase in $S^{6+}/\Sigma S$. Non-buffered $S^{6+}/\Sigma S$ evolution trend (orange) was calculated based on measured/expected S, estimated assuming loss of S^{2-} to a sulfide phase below 6 wt.% MgO. Two model trajectories are shown for 2.5 kbar (grey dotted) and 5 kbar (black dashed), calculated from Eq. 21, with $Fe^{3+}/\Sigma Fe$ and T vs. MgO for the model were derived by simulating isobaric fractional crystallization buffered at FMQ+0.2 in Comagmat 3.72 (Ariskin et al. 2018). The SCSS curve in (a) (orange) in was calculated for the 2.5 kbar model after Fortin et al. (2015).

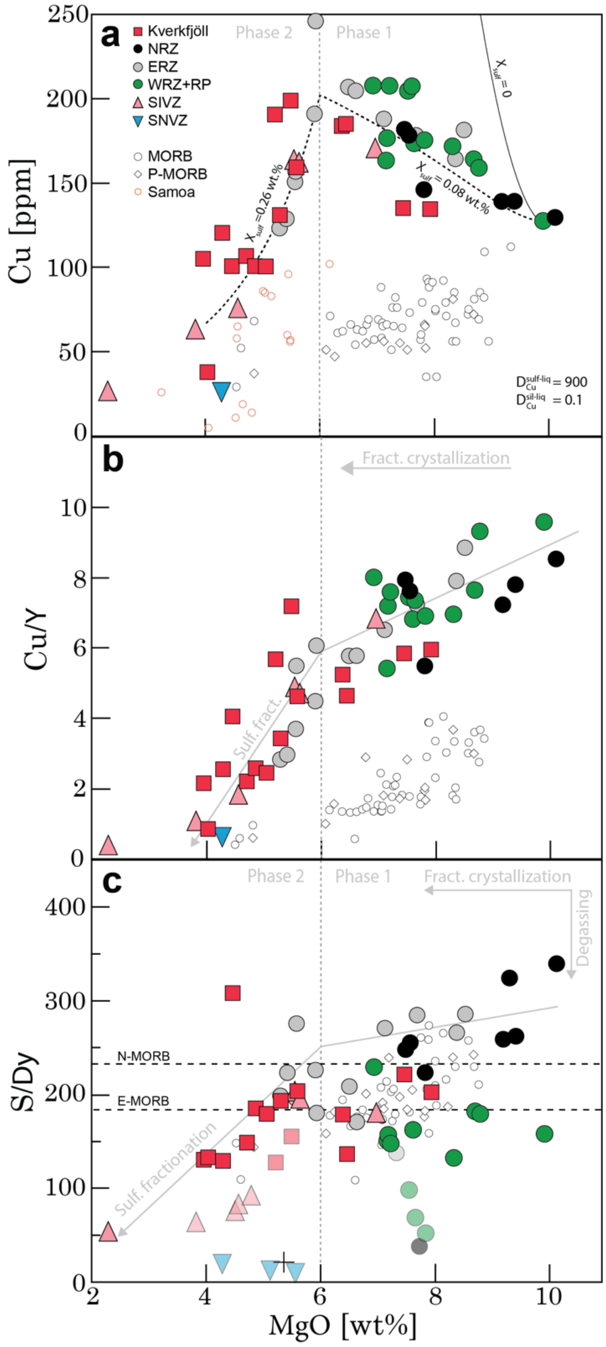

Figure 3 Effect of sulfide melt immiscibility. **(a)** Cu versus MgO. A clear inflection point at MgO ≈ 6 wt.% signals the onset, or acceleration, of sulfide fractionation. The observed trends indicate fractionation of about 0.08 wt.% sulfide melt between MgO = 6–10 wt.% (Phase 1) and 0.26 wt.% between MgO = 4-6 wt.% (Phase 2) (dashed grey line; see Supplementary material for model details). The modelled fractional crystallization trajectory for $X_{sulf} = 0$ (black line) greatly overestimates Cu concentrations. **(b)** Cu/Y versus MgO. Because $D_{Cu}^{sil-liq} \approx D_{Y}^{sil-liq}$, decreasing Cu/Y may indicate slight fractionation of sulfide during Phase 1. **(c)** S/Dy versus MgO. The S/Dy variability in undegassed, primitive (MgO > 6 wt.%) samples suggest either lower S/Dy in the WRZ and Kverkfjöll mantle compared to NRZ and ERZ, or, alternatively, buffering of primitive melt S concentrations during partial melting by mantle sulfides (Ding and Dasgupta 2018). MORB (white circles) data are sourced from Labidi et al. (2012, 2013, 2014) and Labidi and Cartigny (2016). Plume-influenced MORB data (P-MORB) covering the LOMU, Discovery and Shona anomalies in the South Mid-Atlantic Ridge are from Labidi et al. (2013). Samoan (orange circles) data are from Labidi et al. (2015).

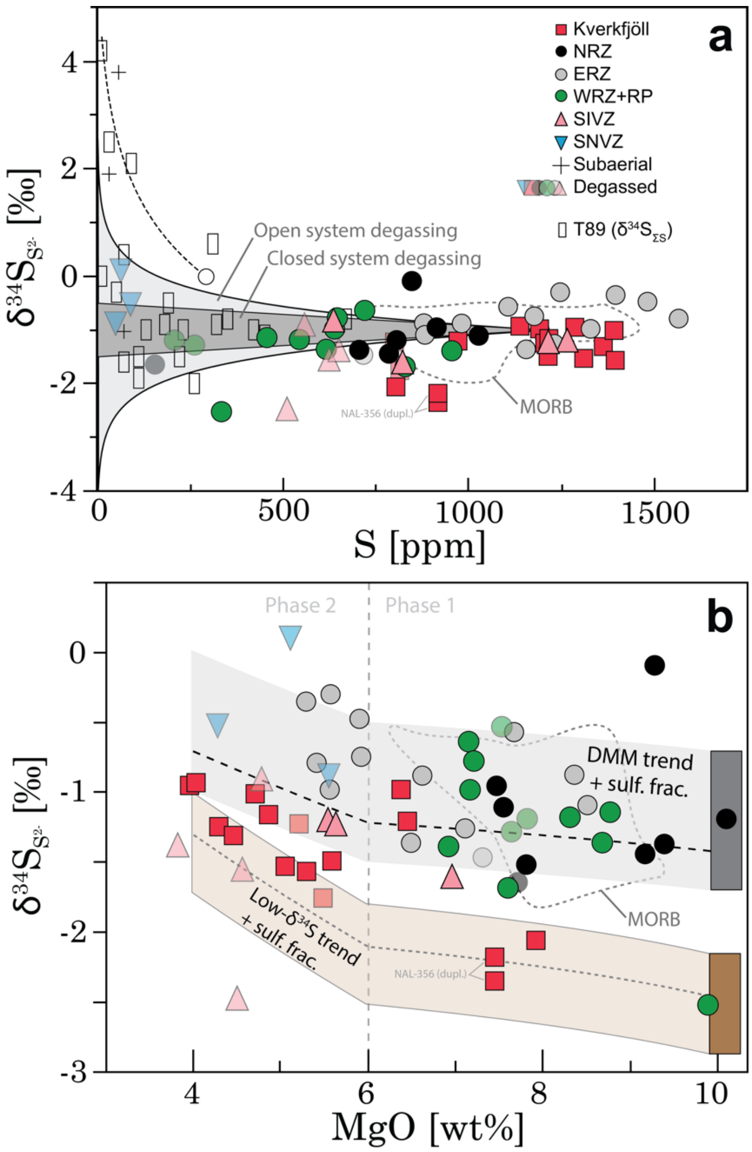

Figure 4 (a) $\delta^{34}S_{S^{2-}}$ versus S concentrations. The effect of degassing on $\delta^{34}S$ in Icelandic samples is clearly illustrated by generally increasing $\delta^{34}S$ at low S concentrations. Large scatter in previously published data on Iceland (white rectangles; T89; Torssander 1989) demonstrates the advantage of using relatively undegassed subglacial glasses for studying pre-eruptive S isotope compositions. All undegassed Icelandic basalts have negative $\delta^{34}S_{S^{2-}}$ values. Shaded fields represent open (light grey) and closed system degassing (dark grey) of a basaltic melt with $\delta^{34}S_{S^{2-}}$ = -1 % and S = 1200 ppm, assuming a fractionation factor of $\Delta^{34}S_{gas-melt}$ = 0±0.5 ‰. Dashed black model line shows the effect open system degassing of a hypothetical undegassed rhyolitic melt with S = 300 ppm (white circle). Model details are explained in the Supplementary Information. **(b)** $\delta^{34}S_{S^{2-}}$ versus MgO. Redox buffering of S following sulfide fractionation may lead to increasingly positive $\delta^{34}S_{S^{2-}}$ values during melt evolution (shaded fields). However, a DMM-like mantle component cannot by itself explain the most negative $\delta^{34}S_{S^{2-}}$ values in the primitive (MgO > 6 wt.%) samples. Instead, an additional mantle component with more negative $\delta^{34}S$ signature is implicated. Modelled $\delta^{34}S_{S^{2-}}$ trajectories for hypothetical DMM (MgO = 10 wt%, $\delta^{34}S_{S^{2-}}$= -1.44 ‰, S = 750 ppm, $S^{6+}/\Sigma S$ = 0.185; similar to NAL-611) and "low-$\delta^{34}S$ component" (MgO = 10 wt%, $\delta^{34}S_{S^{2-}}$ = -2.5 ‰, S = 400 ppm, $S^{6+}/\Sigma S$ = 0.236; similar to MID-1) primary mantle melts are shown by dashed lines. The NRZ sample HS92-15 is an outlier with a clearly less negative $\delta^{34}S$ value of -0.1 ‰ compared to other NRZ samples. Degassed samples are shown for reference (transparent symbols). MORB field drawn from the references given in Fig. 3.

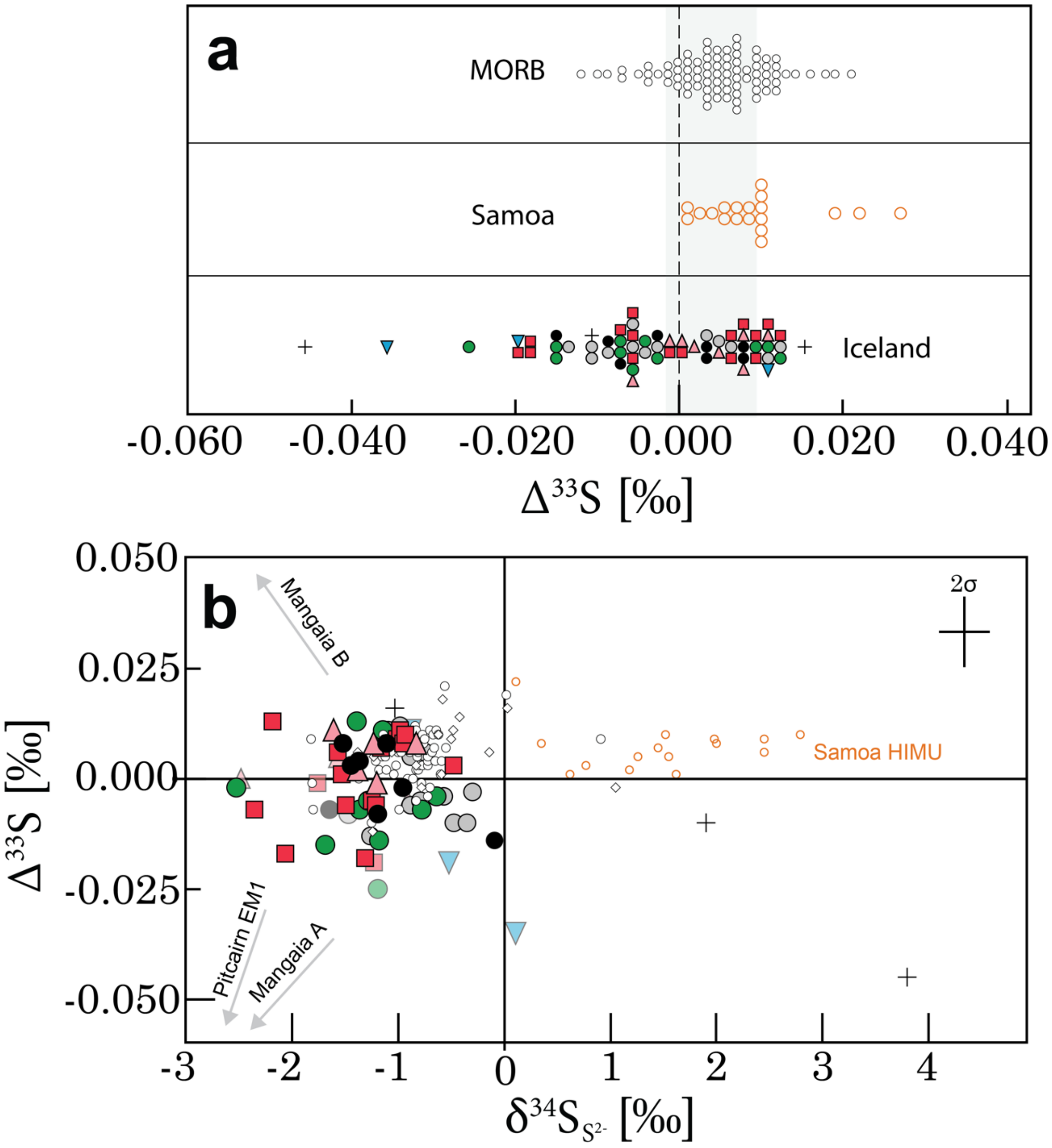

Figure 5 (a) A compilation of basaltic glass-derived $\Delta^{33}S$ data. Iceland samples overlap with MORBs and Samoan OIBs but are shifted toward more negative $\Delta^{33}S$. Negative $\Delta^{33}S$ values in MORBs are uncommon. Grey field shows the MORB average (0.004±0.006, 1σ). **(b)** $\Delta^{33}S$ vs. $\delta^{34}S_{S^{2-}}$ systematics. Available hotspot S isotope data from Iceland, Samoa (orange circles; Labidi et al. 2015; Dottin et al. 2020a), Mangaia and Pitcairn seem to describe a positive correlation between $\Delta^{33}S$ and $\delta^{34}S$ which is also present in the Archaean sediment record (Johnston et al. 2011). However, a break from this trend is represented by the Mangaian HIMU endmember B ($\delta^{34}S$ = -7.5 ‰, $\Delta^{33}S$ = +0.200 ‰; Dottin et al. 2020b). Notably, very few data plot in the 2nd quadrant. Grey arrows point toward the Mangaia HIMU endmember A ($\delta^{34}S$ = -22 ‰, $\Delta^{33}S$ = -0.600 ‰; Cabral et al. 2014) and B and the Pitcairn EM1 component ($\delta^{34}S$ = -6 ‰, $\Delta^{33}S$ = -0.800 ‰; Delavault et al. 2016). Degassed Samoan samples from Dottin et al. (2020), and MORBs that have assimilated seawater sulfate have been filtered out following Labidi et al. (2014). Symbols and MORB data as in Fig. 3.

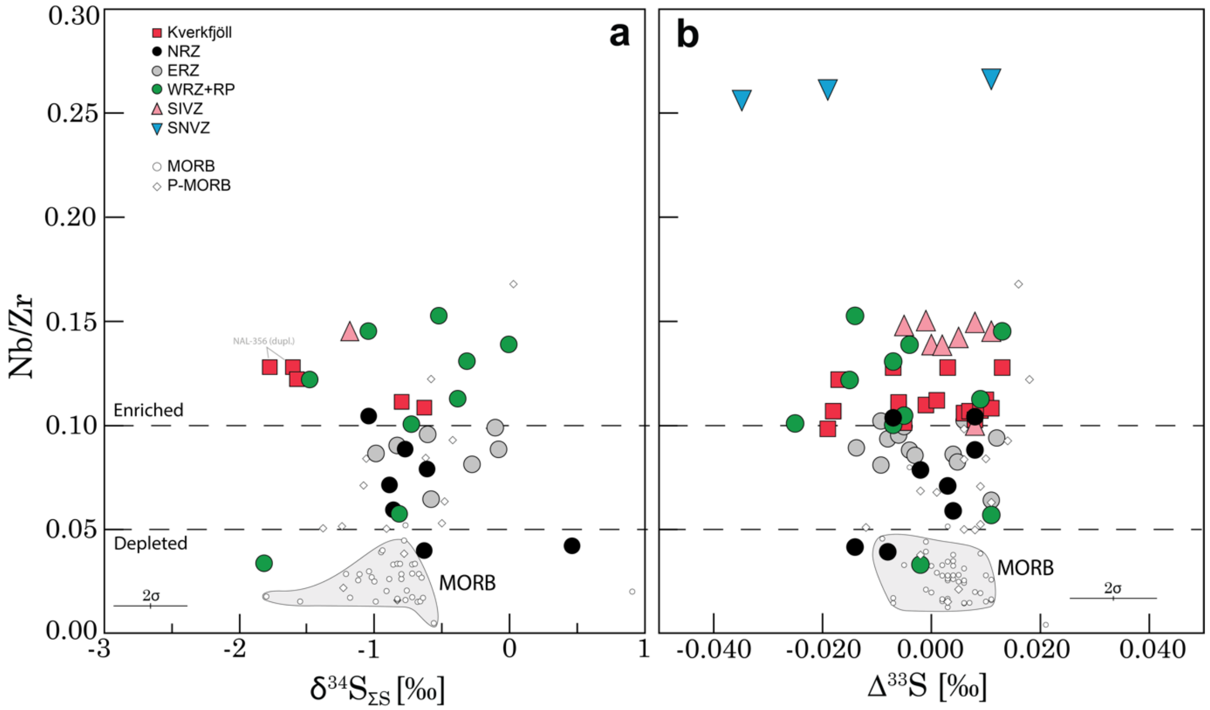

Figure 6 Trace element (Nb/Zr) enrichment vs. **(a)** $\delta^{34}S$ and **(b)** $\Delta^{33}S$. No clear correlation is seen between trace element enrichment, as measured by Nb/Zr, and $\delta^{34}S$ or $\Delta^{33}S$. The greatest variation in $\delta^{34}S$ values is observed in both the depleted ($Nb/Zr < 0.05$) and the enriched glasses ($Nb/Zr > 0.10$), while moderately enriched samples fall within the MORB field (light grey). Both depleted and enriched samples trend toward negative $\Delta^{33}S$ compared to MORBs. Samples that have experienced degassing or considerable sulfide fractionation ($MgO < 6$ wt.%) may have altered $\delta^{34}S$ values and have been filtered out from (a) (see sections 4.1 and 4.2). MORB samples that have assimilated seawater sulfate have been filtered out from (a) following Labidi et al. (2014). The entire dataset is shown in (b), as $\Delta^{33}S$ is not affected by magmatic processes. MORB and P-MORB data as in Fig. 3.

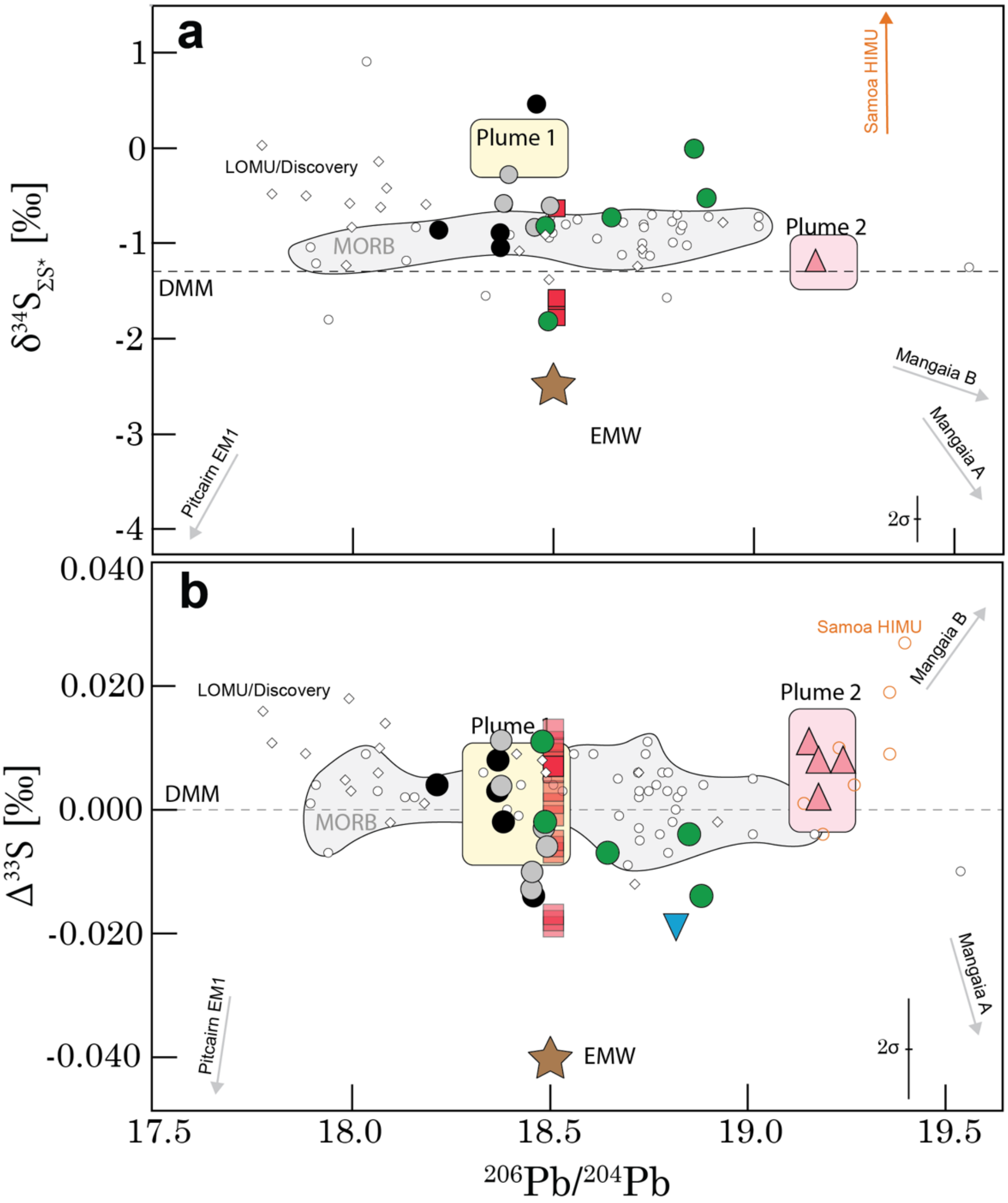

Figure 7 Lead and sulfur isotope relationships. **(a)** $\delta^{34}S_{\Sigma S}$ versus ^{206}Pb/^{204}Pb. The $\delta^{34}S_{\Sigma S}$ values of Icelandic glasses partly overlap with those of MORBs (grey field). Notably, the anomalously negative $\delta^{34}S$ values at Kverkfjöll and the WRZ sample MID-1 are both associated with a ^{206}Pb/^{204}Pb value of ~18.5. **(b)** Icelandic glasses show a greater variability in $\Delta^{33}S$ values compared to MORBs and have overall negative $\Delta^{33}S$ values that seem to converge at the EMW component. Notably, the SIVZ samples, that have the highest ^{206}Pb/^{204}Pb in Iceland (> 19.0) lack anomalous $\Delta^{33}S$ values. Pb isotope data for the Icelandic samples are sourced from Halldórsson et al. (2016a) and Jackson et al. (2020). The value ^{206}Pb/^{204}Pb = 18.508 reported for KVK-77 by Halldórsson et al. (2016a) is assumed for all KVK samples (transparent symbols). EMW = subduction fluid-enriched mantle wedge. Symbols and MORB data as in Fig. 3.

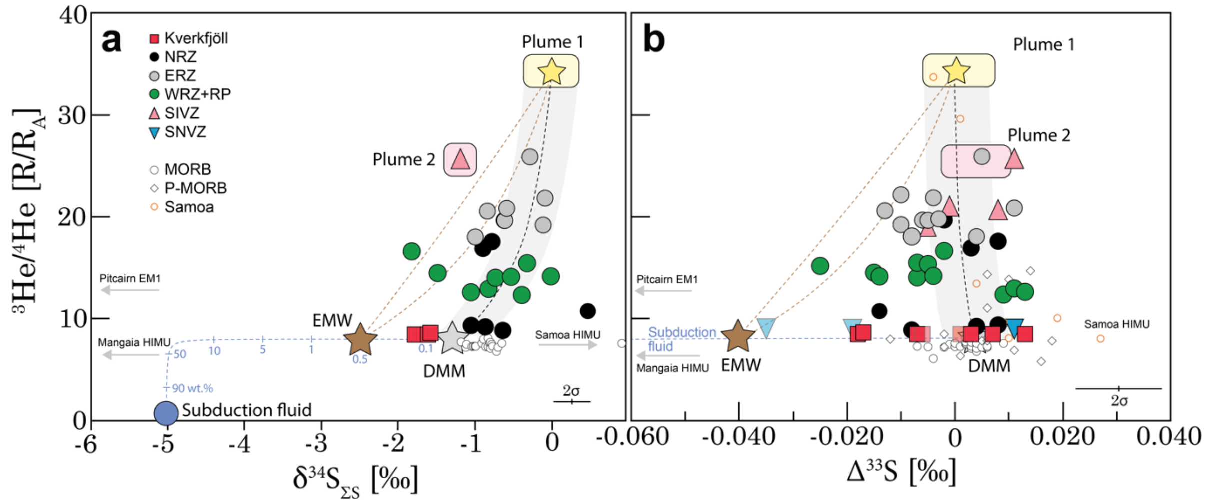

Figure 8 Sulfur and helium isotope relationships. **(a)** The ^{3}He/^{4}He vs. δ^{34}S$_{ΣS}$ systematics of Icelandic lavas can be explained by three-component mixing of DMM (^{3}He/^{4}He = 8 R/R$_A$, δ^{34}S$_{ΣS}$ = -1.3 ‰; grey star), Plume 1 mantle (^{3}He/^{4}He = 33.6 R$_A$, δ^{34}S$_{ΣS}$ = -0.3‰; yellow star) and EMW (subduction fluid-enriched mantle wedge; ^{3}He/^{4}He = 8 R$_A$, δ^{34}S$_{ΣS}$ = -2.5 ‰; brown star). The radiogenic Plume 2 component (cf. Fig. 7) sampled by SIVZ lavas (pink field) has high ^{3}He/^{4}He (~25 R$_A$) and Δ^{33}S ≈ 0 ‰, but its δ^{34}S signature is only constrained by a single sample. The EMW component that gives rise to the low-δ^{34}S and low ^{3}He/^{4}He Kverkfjöll lavas is created by adding ~0.5 wt.% subduction derived fluid (blue circle) with a composition of δ^{34}S$_{ΣS}$ = -5 ‰, S = 9620 ppm, similar to subduction fluids released from metasediments during devolatilization at ~100 km depth (Li et al. 2020). **(b)** ^{3}He/^{4}He versus Δ^{33}S. There is a clear tendency toward negative Δ^{33}S values in Icelandic lavas compared to DMM. This can be explained if the EMW component has a Δ^{33}S value of –0.040 ‰, which requires a subduction fluid component with Δ^{33}S = -0.130 ‰. The Δ^{33}S variability decreases with increasing ^{3}He/^{4}He to values ~0 ‰, which is taken as the Δ^{33}S signature of the Plume 1 component. Two SNVZ (BOTN-1 and OLAF-1) and Kverkfjöll samples (KVK-147 and KVK-168) with degassed ^{3}He/^{4}He are projected to the ^{3}He/^{4}He = 9.0 and 8.5 R$_A$, which are representative of Snæfellsnes and Kverkfjöll lavas and geothermal fluids, respectively (Hardardóttir et al., 2018). Binary mixing curves are shown by dashed lines. Two binary mixing lines between EMW and Plume are shown scenario with [He]$_{\mathrm{Plume1}}$/[He]$_{\mathrm{EMW}}$ of 1 (straight line) and 0.5 (curved line). End-member compositions are given in Table S6. Sample filtering, references and the Mangaia HIMU, Samoa and Pitcairn EM1 compositions as in Fig. 7. Helium isotope data for the Iceland samples from Macpherson et al. (2005), Füri et al. (2010) and Halldórsson et al. (2016b). MORB and P-MORB data as in Fig. 3.

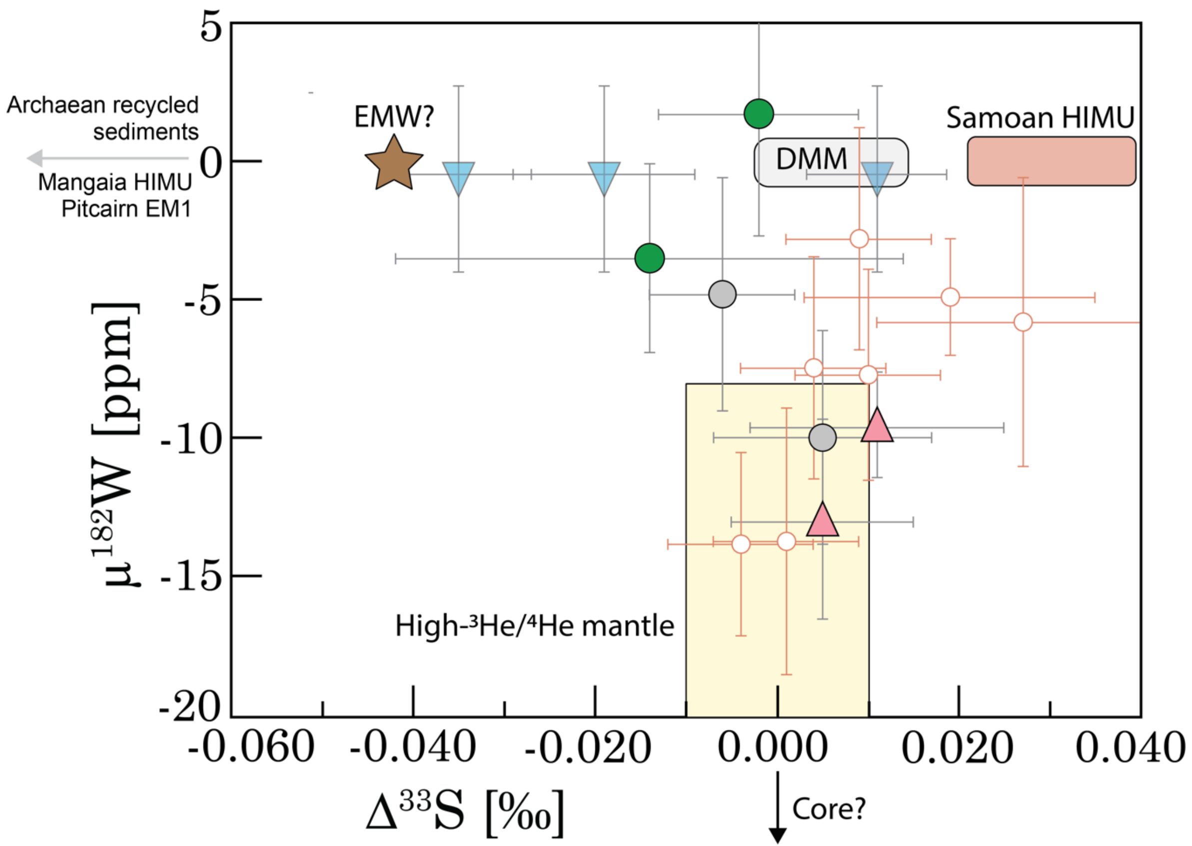

Figure 9 μ^{182}W versus Δ^{33}S. Icelandic and Samoan samples with negative μ^{182}W anomalies, that also have high ^{3}He/^{4}He, converge toward a chondritic Δ^{33}S ≈ 0 ‰, which is taken as a signature of an early-differentiated, primordial mantle reservoir. Samples with μ^{182}W approaching 0 exhibit larger variation in Δ^{33}S, with Icelandic samples pulling toward negative and Samoan toward positive Δ^{33}S values. The μ^{182}W signature of the SNVZ samples is taken as the average of two other SNVZ samples SNS-206 (-0.6 ppm) and SNS-214 (-0.7 ppm) reported by Mundl-Petermeier et al. (2019). The μ^{182}W data for all Iceland samples are sourced from Mundl-Petermeier et al. (2019), except for sample A24 which is from Jackson et al. (2020). Δ^{33}S and μ^{182}W data for Samoa are sourced from Dottin et al. (2020a). Error bars represent 2SE for both μ^{182}W and Δ^{33}S. Arrows point toward Δ^{33}S- μ^{182}W compositions of Mangaia, Pitcairn and Earth's core based on Cabral et al. (2013), Labidi et al. (2013), Delavault et al. (2016) and Mundl et al. (2017). Symbols as in Fig. 3.